

The background is a solid purple color with several abstract geometric elements. A large, semi-transparent circular graphic is centered on the right side, featuring concentric rings and a dotted border. Diagonal lines and a grid of small dots are also visible, creating a technical or scientific aesthetic.

# III-4

Surface and  
Thin Films



BL6U

## Substituent-Induced Intermolecular Interaction in Organic Crystals Revealed by Precise Band-Dispersion Measurements

H. Yamane and N. Kosugi

Department of Photo-Molecular Science, Institute for Molecular Science, Okazaki 444-8585, Japan

Solid-state functionalities of organic molecules are governed not only by individual molecular properties but also by their intermolecular interactions. This concerted interplay dominates a key process of the electric conduction in functional molecular systems. In this work, we have investigated the intermolecular energy-*vs*-momentum  $E(\mathbf{k})$  relation, originating from the molecular stacking periodicity, of sub-100-meV scale in metal phthalocyanine (MPc) crystalline films. The small  $E(\mathbf{k})$  relation of MPc with different terminal groups and central metals are sensitive and essential to characterize the intermolecular interaction in terms of the intermolecular distance, the molecular conformation, and the orbital symmetry.

Figure 1 shows the emission angle ( $\theta$ ) dependence of the angle-resolved photoemission (ARPES) spectra and its intensity map for the flat-lying monolayer and crystalline films of ZnPc on Au(111) at 15 K. For the monolayer, the dispersive and non-dispersive peaks appear around the binding energy ( $E_b$ ) of 0~0.32 eV and 0.74 eV, respectively. The parabolic dispersion at  $E_b = 0\sim 0.32$  eV is derived from the Shockley state (SS) of the Au(111) surface, which is modified by the complex interplay of molecule-substrate interactions. The non-dispersive peak at  $E_b = 0.74$  eV is derived from the highest occupied molecular orbital (HOMO) of C 2p ( $\pi$ ) character in ZnPc. The observed HOMO-peak intensity shows a sharp  $\theta$  dependence with the maximum at  $\theta = 34^\circ$ . This is due to the reflection of the spatial electron distribution of HOMO. For the ZnPc crystalline film, the SS band of Au(111) is suppressed and the HOMO peak is stabilized as  $E_b \sim 1.3$  eV. Since the ZnPc molecule deposited on Au(111) shows the Stranski-Krastanov growth, the quite weak substrate signal of  $E_F$  appears and is utilized for the energy calibration for the precise  $E(\mathbf{k})$  measurement. The  $\theta$  dependence of the HOMO-peak intensity in the ZnPc crystalline film is almost the same as that in the ZnPc monolayer; that is, the molecular orientation indicates the layer-by-layer growth in the crystalline domain and induces orbital delocalization. Indeed, the HOMO peak of the ZnPc crystalline film shows a small dispersive behavior with  $\theta$ . Such a dispersive behavior is not observed in the monolayer film and is related to the delocalized band formation.

In order to investigate the  $\mathbf{k}$  component along the  $\pi$ - $\pi$  stacking direction ( $\mathbf{k}_\perp$ ), we measured the normal emission ARPES as a function of the photon energy ( $h\nu$ ) for crystalline films of various MPc (H<sub>2</sub>Pc, MnPc, CoPc, ZnPc, and F<sub>16</sub>ZnPc) on Au(111) at 15 K. From

this systematic experiment, we revealed quite small but different  $E(\mathbf{k}_\perp)$  relations. The transfer integral ( $t_\perp$ ) of the C 2p band is found to be dependent on the intermolecular distance ( $a_\perp$ ) with the  $75\pm 5$  meV/Å relation (see, Fig. 2). Furthermore, we observed the different dispersion phase and periodicity, depending on the terminal group and central metal in MPc, which originate from the site-specific intermolecular interaction induced by substituents [1].

As described above, precise and systematic  $E(\mathbf{k})$  studies provide deeper insights into the nature of the intermolecular interaction, which further represents the importance of the site specificity in the intermolecular interaction as a possible origin of unique molecular electronic and magnetic properties.

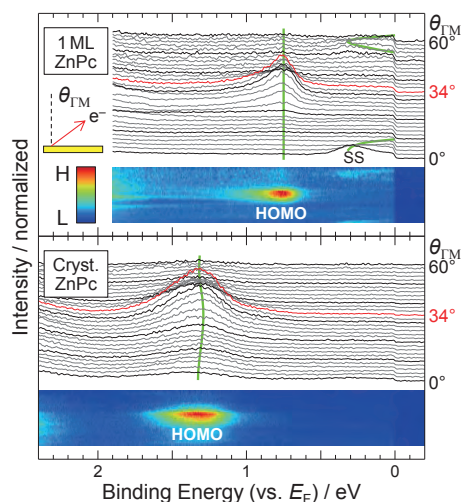


Fig. 1. The  $\theta$  dependence of the ARPES spectra ( $h\nu = 45$  eV) and its intensity map for the monolayer and crystalline films of ZnPc on Au(111) at 15 K.

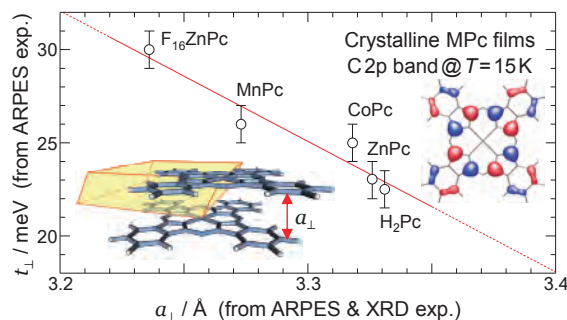


Fig. 2. The  $t_\perp$ -*vs*- $a_\perp$  relation for the C 2p band in MPc crystals at 15 K, with  $t_\perp/a_\perp = 75$  meV/Å line.

[1] H. Yamane and N. Kosugi, Phys. Rev. Lett. **111** (2013) 086602.

BL2A

## Near-Edge X-Ray Absorption Fine Structure Spectroscopic Study of the Annealed Metal Oxide Thin Film

E. Kobayashi<sup>1</sup>, K. K. Bando<sup>2</sup> and T. Okajima<sup>1,3</sup>

<sup>1</sup>Kyushu Synchrotron Light Research Center, Tosu 841-0005, Japan

<sup>2</sup>National Institute of Advanced Industrial Science and Technology, Tsukuba 305-8565, Japan

<sup>3</sup>Research Center for Synchrotron light applications, Kyushu University, Kasuga 816-8580, Japan

Metal oxide is an important material from a fundamental physical point of view and is widely used in the field. It is recognized that the surface structure and surface chemical states are important for applications because it can significantly affect the material characteristics. In this study, the annealing behavior of surface chemical states on Magnesium oxide (MgO) thin film was studied by using near-edge X-ray absorption fine structure (NEXAFS). MgO plays a prototype of metal oxides and is also a wide-gap insulator [1]. In addition, MgO is widely used in the field of catalytic, optical and electrical applications [2, 3].

Mg *K*-edge NEXAFS spectra of MgO thin film on Si(100) wafer (MgO/Si) were measured at the beamline 2A of the UVSOR in the Institute of Molecular Science. MgO thin films of about 10 nm in thickness were prepared by RF magnetron sputtering. The NEXAFS spectra were obtained using the total electron yield (TEY) mode and the partial fluorescence yield (PFY) mode at room temperature. The incident angle of the synchrotron radiation was 0° from the surface normal. The spectra were normalized to the incident photon flux, recorded as a photocurrent at a photon-flux monitor consisting of a gold-evaporated mesh.

The MgO/Si thin film was annealed at several temperatures with 373 K ~ 833 K of 10<sup>-5</sup> ~ 10<sup>-6</sup> Pa order in vacuum. After the annealing, the film was slow cooled in vacuum.

Figure 1 shows the Mg *K*-edge NEXAFS spectra of MgO/Si before and after annealing obtained from PFY mode. Three strong peaks are observed at around 1309.1 eV (A), 1314.7 eV (B) and 1316.9 eV (C), respectively. The spectral features are similar to the experimentally obtained for polycrystalline MgO [4]. However, the intensity ratio of peak A, peak B and peak C change gradually with a rise in annealing temperature. Similar changes were also observed in TEY spectrum.

According to first-principles density functional calculations, the intensity of peak C is stronger than peak B. It is considered that the carbonate and hydroxide on the thin film surface was decomposed and desorbed by heating, the crystallinity of the thin film was improved.

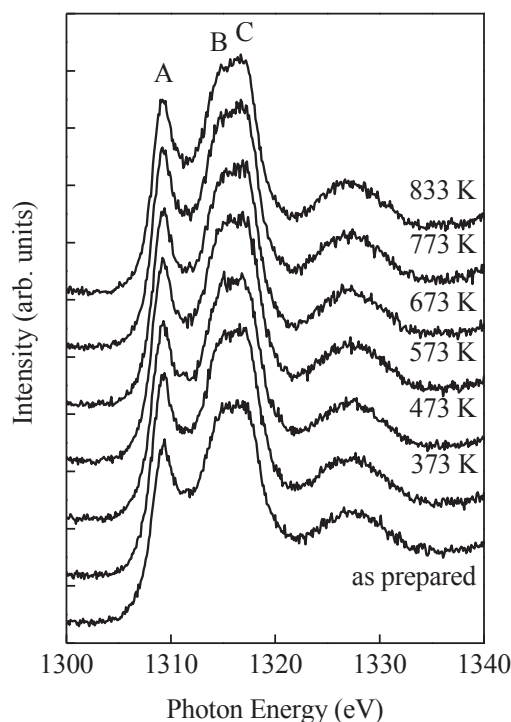


Fig. 1. Mg *K*-edge NEXAFS spectra of MgO/Si before and after annealing obtained from PFY mode.

[1] D. M. Roessler and W. C. Walker, *Phys. Rev.* **159** (1967) 733.

[2] E. A. Colbourn, *Surf. Sci. Rep.* **15** (1992) 281.

[3] G. H. Rosenblatt *et al.*, M. W. Rowe, G. P. Williams, Jr., R. T. Williams, and Y. Chen, *Phys. Rev. B* **39** (1989) 10309.

[4] P. Luches, S. D. Addato, S. Valeri, E. Groppo, C. Prestipino, C. Lamberti and F. Boscherini, *Phys. Rev. B* **69** (2004) 045412.

BL3U

## *In Situ* Observation of Nickel-Borate Catalyst for Oxygen Evolution Reaction by Soft X-Ray Electrochemical XAFS

M. Yoshida<sup>1</sup>, M. Nagasaka<sup>2</sup>, T. Iida<sup>1</sup>, T. Mineo<sup>1</sup>, T. Yomogida<sup>1</sup>, H. Yuzawa<sup>2</sup>,  
N. Kosugi<sup>2</sup> and H. Kondoh<sup>1</sup>

<sup>1</sup>Department of Chemistry, Keio University, Yokohama 223-8522, Japan

<sup>2</sup>Department of Photo-Molecular Science, Institute for Molecular Science, Okazaki 444-8585, Japan

Electrochemical hydrogen production from water has attracted considerable attention due to the potential toward highly efficient energy conversion. This reaction consists of two half reactions of hydrogen and oxygen evolution. However, the efficiency of oxygen evolution reaction (OER) is insufficient for many electrode materials because of the high overpotentials. Recently, Bediako *et al.* reported that a nickel-borate thin film can function as an efficient electrocatalyst for OER and the activity was likely to be dependent on the concentration of potassium borate ( $\text{KB}_i$ ) in electrolyte aqueous solution [1]. Therefore, in this study, the nickel-borate thin film was investigated by *in situ* O *K*-edge XAFS measurements under potential control conditions with changing the electrolyte aqueous solution.

The soft X-ray electrochemical XAFS measurements were performed with the transmission mode at BL3U of UVSOR, according to the previous works [2]. Au/Cr/SiC thin film substrates were used as working electrodes. A home-made electrochemical cell was used with a Pt mesh counter electrode and a Ag/AgCl (saturated KCl) reference electrode.

O *K*-edge XAFS spectra were taken for the electrodeposition reaction of nickel-borate thin film at 1.0 V vs. Ag/AgCl in a 0.1 M  $\text{KB}_i$  aqueous solution containing 0.4 mM  $\text{Ni}(\text{NO}_3)_2$ , as shown in Fig. 1. A peak associated with oxygen species was observed at ca. 528.5 eV and kept to grow for 90 min. Next, the electrolyte solution was changed to 0.5 M  $\text{KB}_i$  aqueous solution without nickel ions and the XAFS measurements were tested with changing the applied electrode potential (Fig. 2). The peak at ca. 528.5 eV disappeared at the lower potential (0.5 V) and regenerated at the higher potential (1.0 V) accompanying with the OER activity. In previous works of Ni *K*-edge XAFS [1], it is indicated that the nickel borate electrocatalyst forms  $\mu$ -oxo/hydroxo nickel centers organized into higher-order domains of edge sharing  $\text{NiO}_6$  octahedra at the higher potential. Thus, our present study demonstrated the presence of the  $\text{NiO}_6$  octahedra domain by the direct observation of oxygen species in the nickel borate thin film. When the concentration of  $\text{KB}_i$  in electrolyte solution decreased, the XAFS peak was not observed even at 1.0 V accompanying with the decrease of the OER activity, which indicates that the formation of the

$\text{NiO}_6$  octahedra domain was suppressed. Therefore, we found that the high activity of nickel borate thin film for OER is derived from the formation of the  $\text{NiO}_6$  octahedra domain and related with the  $\text{KB}_i$  concentration in the electrolyte aqueous solution.

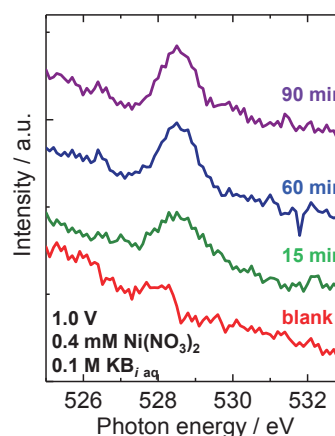


Fig. 1. Time course of *in situ* O *K*-edge XAFS spectra during electrodeposition reaction of nickel-borate thin film.

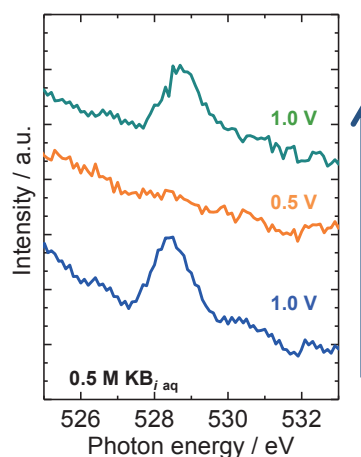


Fig. 2. *In situ* O *K*-edge XAFS spectra under electrochemical control in 0.5 M  $\text{KB}_i$  aqueous solution.

[1] D. K. Bediako *et al.*, *J. Am. Chem. Soc.* **134** (2012) 6801., **135** (2013) 3662.

[2] M. Nagasaka *et al.*, *J. Electron. Spectrosc. Relat. Phenom.* **177** (2010) 130., *J. Phys. Chem. C* **117** (2013) 16343.

BL3U

## Polarized NEXAFS Study on Structure of Nitrogen Doped Rutile $\text{TiO}_2(110)$

 Y. Monya<sup>1</sup>, M. Yoshida<sup>1</sup>, M. Nagasaka<sup>2</sup>, H. Yamane<sup>2</sup>, N. Kosugi<sup>2</sup> and H. Kondoh<sup>1</sup>
<sup>1</sup>Graduate School of Science and Technology, Keio University, Yokohama 223-8522, Japan

<sup>2</sup>Institute for Molecular Science, Okazaki 444-8585, Japan

Nitrogen doped  $\text{TiO}_2$ , which is one of most promising visible-light-response photocatalysts, has been extensively studied to understand the mechanism of its visible-light-response. Although many structural studies on nitrogen dopants in  $\text{TiO}_2$  have been conducted with various techniques, neither doping site nor chemical state of the nitrogen dopant is known in detail. In this work, we measured polarized NEXAFS spectra for nitrogen doped rutile  $\text{TiO}_2(110)$  to elucidate its structure.

The samples were prepared by heating rutile  $\text{TiO}_2(110)$  substrates under  $\text{NH}_3$  atmosphere at 1.0 Torr. Polarized NEXAFS measurements were performed at BL3U with using the partial electron yield method. The photon energies were calibrated by the energy of the first peak (530.6 eV) at O-K edge.

Figure 1 shows O-K edge NEXAFS spectra of rutile  $\text{TiO}_2(110)$  with different polarization directions. For example, NI [001] indicates that x-ray incidence angle is  $90^\circ$  from the surface parallel and its electric vector is lying along the [001] direction (see Fig. 2). In the grazing incidence (GI) geometry, the incidence angle was  $30^\circ$ . For the O-K edge spectra, we observe five peaks (*a-e*) and they are seen in the typical spectra of rutile  $\text{TiO}_2(110)$ . Considering the previous assignments for these peaks [1, 2], peaks *a* and *b* can be attributed to excitations to unoccupied states: ( $\text{Ti } 3d + \text{O } 2p\pi$ ) and ( $\text{Ti } 3d + \text{O } 2p\sigma$ ), respectively. Peaks *c-e* are assigned to ( $\text{Ti } 4sp + \text{O } 2p$ ). In NI[001] spectrum, peak *b* exhibits different polarization dependence from the other peaks. It might be because part of peak *b* is associated with a surface oxygen species shown in Fig. 2. Considering its bonding direction, the excitation to an unoccupied state of ( $\text{Ti } 3d + \text{O } 2p\sigma$ ) character for surface oxygen should be observed only in the [001] direction and particularly strong in NI[001]. Therefore, it can be said that the N doped rutile  $\text{TiO}_2(110)$  has a similar structure to pristine  $\text{TiO}_2$  and the surface oxygen species bridging two Ti atoms remain after doping reactions. Figure 3 shows N-K edge NEXAFS spectra of the nitrogen dopants in the rutile  $\text{TiO}_2(110)$ , where the incidence angle was  $15^\circ$  for GI and  $90^\circ$  for NI from the surface parallel. As a result, seven peaks (*a'-d'* and X, Y, Z) were observed. Peak *a'* and *b'* can be attributed to excitations to unoccupied states: ( $\text{Ti } 3d + \text{N } 2p\pi$ ) and ( $\text{Ti } 3d + \text{N } 2p\sigma$ ), respectively. Peaks *c'* and *d'* are assigned to ( $\text{Ti } 4sp + \text{N } 2p$ ). From these results, the doped N species are likely to occupy the lattice oxygen sites via substitution. It should be noted that peaks X, Y, Z appear exclusively in the N-K edge spectra. Based on the results of XPS, DFT calculations and a previous report [3], it is proposed

that the nitrogen dopants are not only in the form of N but also in the form of NH. Thus, peaks X and Y can be attributed to excitations to NH-derived unoccupied states. Peak Z could be associated with an edge structure.

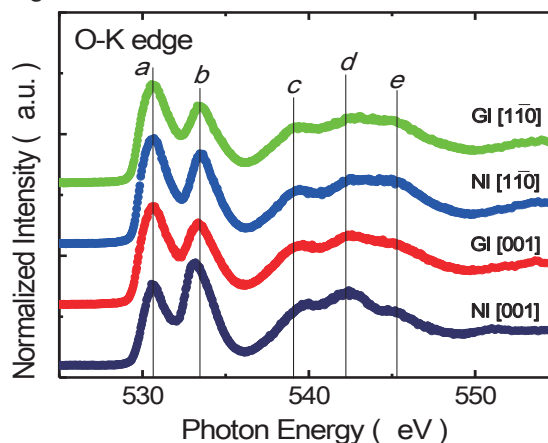


Fig. 1. O-K NEXAFS spectra of N doped rutile  $\text{TiO}_2(110)$ .

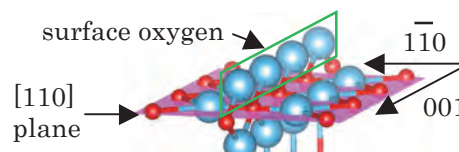


Fig. 2. Structure model for rutile  $\text{TiO}_2(110)$  surface.

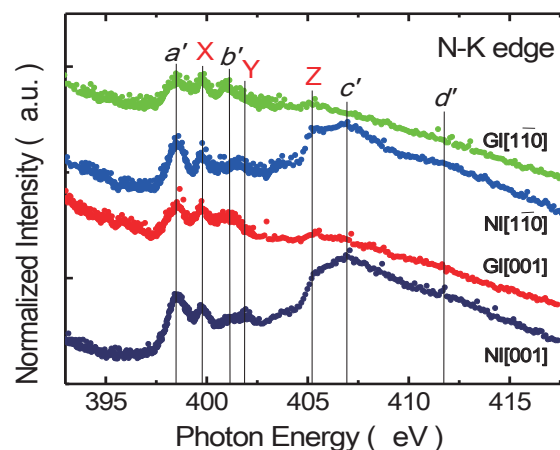


Fig. 3. N-K NEXAFS spectra of nitrogen dopants in rutile  $\text{TiO}_2(110)$ .

- [1] J. G. Chen, Surf. Sci. Rep. **30** (1997) 1.
- [2] E. Filatova *et al.*, Phys. Status Solidi B **246** (2009) No.7, 1454.
- [3] Y. Kim *et al.*, J. Phys. Chem. C **115** (2011) 18618.

BL4B

## Perpendicular Magnetic Anisotropy in Ultrathin Fe Film on MgO Studied by Angular-Dependent X-Ray Magnetic Circular Dichroism

J. Okabayashi<sup>1</sup>, J. W. Koo<sup>2</sup>, H. Sukegawa<sup>2</sup>, S. Mitani<sup>2</sup>, Y. Takagi<sup>3</sup> and T. Yokoyama<sup>3</sup>

<sup>1</sup>Research Center for Spectrochemistry, The University of Tokyo, Tokyo 113-0033, Japan

<sup>2</sup>National Institute for Materials Science (NIMS), Tsukuba 305-0047, Japan

<sup>3</sup>Institute of Molecular Science, Okazaki 444-8585, Japan

Perpendicular magnetization is one of the crucial issues in spintronics research field because it has benefits for thermal stability enhancement and the low current magnetization switching, which are very important for the development of spintronics devices. MgO-based magnetic tunnel junctions have been developed by exploiting the strong perpendicular magnetic anisotropy (PMA) at the interfaces between MgO and CoFeB transition metal alloys, measuring  $2.1 \times 10^5 \text{ J/m}^3$  [1], which is comparable to PMA in Co/Pt multilayers. As a fundamental understanding of PMA induced at the interface between ferromagnetic layer and MgO barrier layer, the electronic and magnetic structures of interfaces between ultrathin Fe layer and MgO have to be clarified explicitly [2]. It brings the understanding for the origin of FeCo alloys on MgO [3]. In order to investigate PMA energy ( $K$ ), it is necessary to evaluate the orbital magnetic moments along parallel and perpendicular directions to the surface. Here, we report the anisotropic orbital moments of Fe/MgO by using angular dependent x-ray magnetic circular dichroism (XMCD).

Samples were grown by electron-beam evaporation methods on MgO substrates. The 0.7-nm-thick Fe layer was deposited on Cr buffer layer and MgO layer was also grown on thin Fe layer. Post annealing at 450 °C was performed to enhance PMA, which was estimated to be  $1.4 \text{ MJ/m}^3$  by vibrating sample magnetometer (VSM) at room temperature [2]. Saturation magnetic field of 0.7 nm Fe layer on MgO was estimated to be 2 T. XMCD measurements were done at UVSOR BL-4B under the conditions of 5 K [4]. Circular polarization was evaluated to be 71%. A magnetic field of 5 T using superconducting magnet was applied along the incident polarized soft x-ray, which is enough to saturate the magnetization along magnetically hard axis direction. The total electron yield mode was adopted. Normal incidence (NI) and grazing incidence (GI) geometries were employed to deduce the anisotropic orbital magnetic moments.

Figure 1 shows Fe  $L$ -edge x-ray absorption spectra and XMCD. Clear metallic peaks in absorption spectra reveal no mixing with oxygen atoms. XMCD spectra in NI and GI setups reveal the difference in  $L_3$  edges, suggesting that the large orbital moments are induced in NI geometry. Using orbital sum rules, 0.22 and  $0.17 \mu_B$  are estimated for NI and GI geometries, respectively. Considering the Bruno relationship;

$K = (\xi/4)\Delta m_l$ , where  $\xi$  is spin-orbit coupling, we obtain  $K = 0.9 \text{ MJ/m}^3$ , which is comparable to the results obtained by VSM. We note that VSM measurements at low temperature are difficult due to the diamagnetic contribution from MgO substrates. Therefore, element specific XMCD measurements become a unique technique for probing ultrathin magnetic layer on MgO.

Considering above results, the origin of PMA in Fe/MgO interface can be understood by the anisotropic orbital moments induced by spin-orbit interaction at the interface. Fe  $3d_{z^2}$  states are pushed up above the Fermi level through the hybridization with O  $2p_z$  orbitals and large perpendicular orbital moments are induced. Therefore, we conclude that anisotropic orbital moments are the origin of large PMA in Fe/MgO interface.

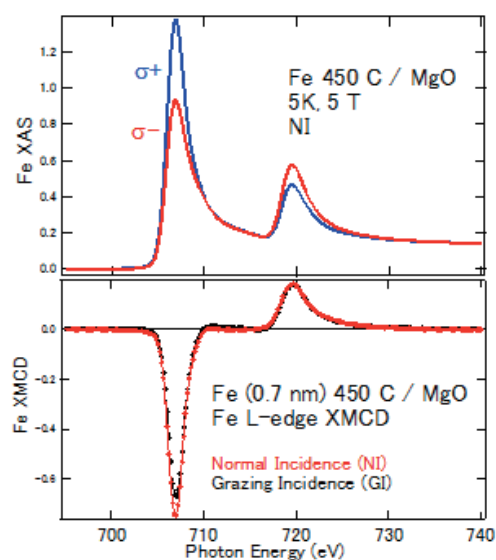


Fig. 1. X-ray absorption spectra of NI and XMCD of both NI and GI setups in Fe/MgO at 5 K and 5 T.

- [1] S. Ikeda *et al.*, Nature Mater. **9** (2010) 721.  
 [2] J. W. Koo *et al.*, Appl. Phys. Lett. **103** (2013) 192401.  
 [3] J. Okabayashi *et al.*, Appl. Phys. Lett. **103** (2013) 102402.  
 [4] T. Yokoyama *et al.*, Int. Rev. Phys. Chem. **27** (2008) 449.

BL4B

## XAS Study of Magnetic Atoms on Pb/Ge(111)

S. Hatta, N. Sakata, H. Okuyama and T. Aruga

Graduate School of Science, Kyoto University, Kyoto 606-8502, Japan

The Pb monolayer on Ge(111) has surface states exhibiting spin splitting due to the Rashba spin-orbit interaction [1, 2]. One of the spin-split surface states makes spin-polarized Fermi surfaces with the spin splitting of 200 meV. Our four-point-probe conductivity measurements of the monolayer demonstrated the metallic temperature dependence of the conductivity and the high conductivity of  $\sim 10$  mS. Therefore the monolayer is actually suitable to study the role of the spin-orbit interaction and spin polarization of two-dimensional states in electron transport. Recently, the spin-orbit interaction is expected to have a significant effect in the coupling with conduction electrons and a local magnetic moment, resulting in the increase or decrease of the Kondo temperature [3, 4]. In order to address such an issue, we have investigated the magnetic properties of Co and Fe atoms adsorbed on the Pb monolayer.

We performed X-ray absorption spectroscopy (XAS) experiments at BL4B using the x-ray magnetic circular dichroism (XMCD) end station. The Ge(111) substrate was cleaned by cycles of annealing and Ar ion sputtering until a sharp  $c(2\times 8)$  low-energy electron diffraction (LEED) pattern was observed. The Pb deposition of  $\sim 3$  ML was done from an alumina crucible heated by tungsten loops, followed by annealing at 550 K. Figure 1 shows the obtained  $(\sqrt{3}\times\sqrt{3})R30^\circ$  LEED pattern of the Pb monolayer. A small amount of Co or Fe was evaporated by electron bombardment with a rate of  $\sim 0.005$  ML/sec. Immediately after the deposition on the room temperature Pb/Ge(111) surface, the sample was transferred to the XMCD chamber and cooled down to 6 K.

Figures 2 show  $L_{2,3}$ -edge XAS spectra of Co (0.22 ML) on Pb/Ge(111) at  $\pm 1$  T and the incidence angles of  $0^\circ$  and  $55^\circ$  from the surface normal. The broad feature of the adsorption peaks seemed to be unchanged from 0.07 to 0.22 ML. This indicates the significant interaction between the Co 3d and surface states. For XMCD, unexpectedly little signal was observed both at normal and grazing incidence, as shown in Fig. 2. It was same in the measurements with  $\pm 3$ T. This result shows that the magnetic moment of the adsorbed Co atoms is quenched. On the other hand, a XMCD signal was observed for Fe (0.17 ML) on Pb/Ge(111). The magnetic field and the incidence angle dependence of the XMCD signal was found. We are proceeding with further analysis of the magnetic moments of the adsorbed Fe atoms.

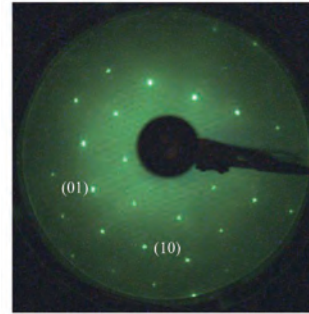


Fig. 1. A  $(\sqrt{3}\times\sqrt{3})R30^\circ$  LEED pattern observed for the Pb monolayer on Ge(111) ( $E_p=90$  eV).

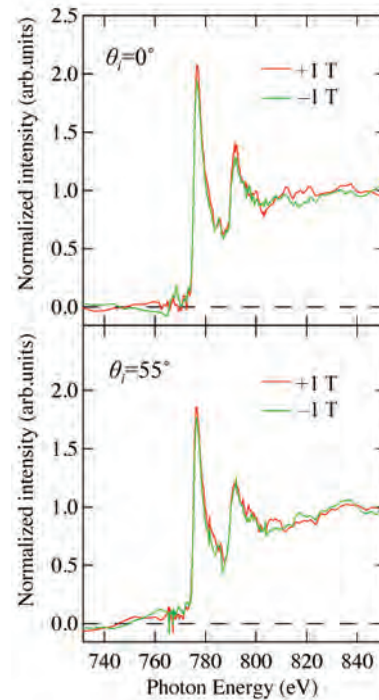


Fig. 2.  $L_{2,3}$ -edge XAS spectra of Co (0.22 ML) on the Pb/Ge(111) recorded at 6 K and  $\pm 1$  T.

- [1] K. Yaji *et al.*, Nat. Comm. **1** (2010) 17.
- [2] K. Yaji *et al.*, Phys. Rev. B **86** (2012) 235317.
- [3] M. Zarea, S. E. Ulloa and N. Sandler, Phys. Rev. Lett. **108** (2012) 046601.
- [4] T. Yanagisawa, J. Phys. Soc. Jpn. **81** (2012) 094713.

BL4B

## Study on Magnetic Properties of Metal-Coordinated Phthalocyanine Molecules Self-Assembled on Semiconductor Surface Reconstructions

T. Uchihashi and S. Yoshizawa

International Center for Materials Nanoarchitectonics (MANA), National Institute for Materials Science, Tsukuba 305-0044, Japan

Thin film complex molecules fabricated by thermal evaporation onto a metal surface have been extensively studied using X-ray absorption spectroscopy (XAS) and X-ray magnetic circular dichroism (XMCD) for the purpose of device applications [1]. In this work, we studied the magnetic properties of Co-Phthalocyanine (Pc) and MnPc self-assembled on the Si(111)-( $\sqrt{7}\times\sqrt{3}$ )-In surface reconstruction [referred to as ( $\sqrt{7}\times\sqrt{3}$ )-In], which is made of monatomic indium layers on a clean silicon surface. Since the ( $\sqrt{7}\times\sqrt{3}$ )-In surface exhibits superconducting phase transition at 3 K [2], interesting competition effects between superconductivity and magnetism are expected to occur in this system.

The experiment was performed in the ultrahigh vacuum XMCD system with a superconducting magnet, which was set at the UVSOR beam line BL4B in the Institute for Molecular Science. Figure 1 shows the LEED patterns of the ( $\sqrt{7}\times\sqrt{3}$ )-In surface before (left) and after (right) MnPc was evaporated to a monolayer level. High crystallinity was confirmed for both cases. Similar results were obtained for CoPc/( $\sqrt{7}\times\sqrt{3}$ )-In. XMCD spectra were determined from the difference between the XAS spectra taken at  $B = \pm 5$  T.

For the CoPc/( $\sqrt{7}\times\sqrt{3}$ )-In sample, no XMCD signal was obtained. Since CoPc has a spin 1/2 at the Co atom in a free state, this spin must be quenched, for example, by charge transfer between the molecule and the substrate. In contrast, clear XMCD signals were obtained for the MnPc/( $\sqrt{7}\times\sqrt{3}$ )-In sample (see Fig. 2). This clearly indicates that spins in the Mn atom still survive when the molecule is adsorbed on this surface. These behaviors are similar to the ones observed for their adsorption on noble metal surfaces.

According to our recent experiments, superconducting energy gap is retained on the first and the second layers of CoPc on ( $\sqrt{7}\times\sqrt{3}$ )-In. This is consistent with our observation that the spin of CoPc is quenched on absorption. On the other hand, the spins surviving in the MnPc molecule can suppress the superconductivity of the ( $\sqrt{7}\times\sqrt{3}$ )-In surface. This will be further studied by combining the XMCD experiment, STM, and electron transport measurement.

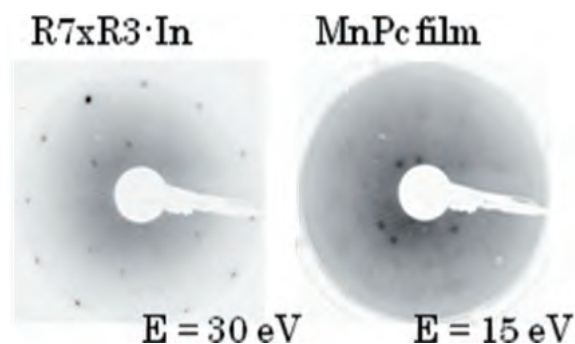


Fig. 1. LEED patterns of the CoPc/( $\sqrt{7}\times\sqrt{3}$ )-In sample.

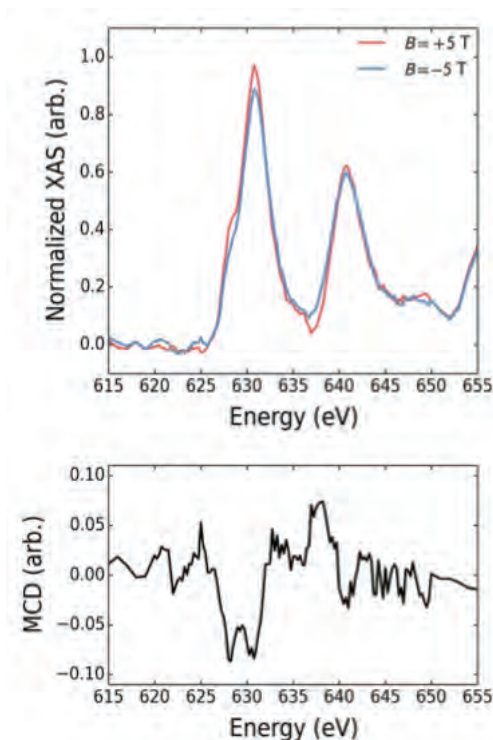


Fig. 2. XAS and XMCD spectra of the CoPc/( $\sqrt{7}\times\sqrt{3}$ )-In sample taken at the incident angle  $\theta = 0$ .

[1] Y. Takagi *et al.*, UVSOR ACTIVITY REPORT **38** (2011) 67.

[2] T. Uchihashi *et al.*, Phys. Rev. Lett., **107** (2011) 207001.

BL4B

## Magnetic Linear Dichroism Study of Non-Ferromagnetic Co on W(110)

H. Nakano<sup>1</sup>, T. Nakagawa<sup>2</sup>, K. Eguchi<sup>1</sup>, N. Takagi<sup>1</sup> and T. Yokoyama<sup>1</sup>

<sup>1</sup>*Institute for Molecular Science, Okazaki 444-8585, Japan*

<sup>2</sup>*Department of Molecular and Material Sciences, Kyushu University, Kasuga 816-8580, Japan*

Metallic Co is known as a robust ferromagnetic material, irrespective of its crystal structures and pressure. Thus antiferromagnetic phase of Co has not been found so far both for bulk and thin films. However, the magnetism of Co single layer grown on refractory metals, W and Mo, has been a puzzling issue since no evidence of magnetic ordering has been found [1]. On the other hand, Fe, a typical ferromagnetic material at ambient conditions, shows variety of magnetic phases such as ferromagnetic, antiferromagnetic, spin density waves, depending on the crystal structure, lattice constant, and thickness. Here we report non parallel alignment of Co magnetic moment proved by x-ray magnetic linear dichroism (XMLD).

Experiments were done in a x-ray magnetic circular dichroism (XMCD) chamber with superconducting magnet ( $H \sim 6$  T). Co was deposited on W(110), which was cleaned by repeated cycles of oxidation and high temperature flash upto 2200 K. The x-ray linear dichroism (XLD) was measured with the polarization of the light fixed and the azimuthal angle of the crystal rotated.

Figure 1(a) shows XMCD spectra taken on single layer Co grown on W(110) at  $T_s = 5$  K and a magnetic field of 5 T. The spectra for the parallel and antiparallel alignment between the light helicity and the magnetic field are nearly identical, indicating the disappearance of the macroscopic spin moments. The zero spin magnetic moment obtained in XMCD has several scenarios. One is the non-parallel alignment of the spin moment such as antiferromagnetic structure so as to give the macroscopic zero moment, and another is the missing of the magnetic moment in Co due to the strong hybridization with W substrate.

Linear dichroism could be observed for non-parallel alignment of the magnetic moment owing to the asymmetry of the magnetic structure. Figure 1(b) shows XLD spectra taken between 5 K and 60 K, where the dichroic signal is shown as the difference between the light polarization ( $E$ ) // [110] and  $E$  // [001] directions. In Fig. 1(c) the XMLD intensity is largest at  $T_s = 5$  K, and decreases with increasing the temperature. Above 20 K, the XMLD stays at the almost constant value, which comes from  $C_2$  symmetry of Co/W(110) and the instrumental asymmetry. The temperature dependence of the XLD suggests an additional ordering below 20 K.

It is unlikely that the Co magnetic moment adjacent to W atoms vanishes due to the strong banding. Since the thickness dependence of Co magnetic moment (not shown) demonstrates a rapid increase above 1

ML Co thickness and recover to  $\sim 80\%$  of bulk Co spin moment at 2 ML, which cannot be explained by the zero magnetic moment in the first Co layer.

In summary, we show for the first time that the monolayer Co on W(110) is not non-magnetic, but it exhibits the non-parallel alignment of the magnetic moment, which cancels with each other such as an antiferromagnetic structure.

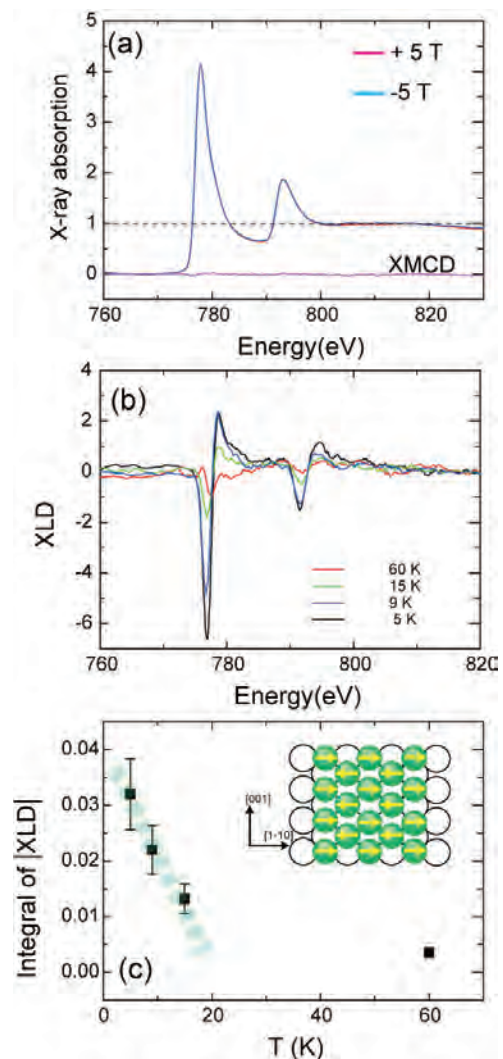


Fig. 1. (a) XAS and XMCD spectra for 0.6 ML Co on W(110) at  $T_s = 5$  K. (b) Temperature dependent XLD spectra for 0.6 ML Co on W(110). (c) XMLD intensity as a function of temperature. The inset is a schematic drawing of the Co spin structure.

[1] G. Garreau, M. Farle, E. Beaurepaire and K. Baberschke, Phys. Rev. B **55** (1997) 330.

BL4B

## Magnetic Property of Vanadyl Phthalocyanine on Ferromagnetic Iron Surface Studied by XMCD

K. Eguchi<sup>1</sup>, Y. Takagi<sup>1,2</sup>, T. Nakagawa<sup>1,2</sup> and T. Yokoyama<sup>1,2</sup>

<sup>1</sup> The Graduate University for Advanced Studies (SOKENDAI), Okazaki 444-8585, Japan

<sup>2</sup> Institute for Molecular Science, Okazaki 444-8585, Japan

It is important to understand the magnetic interactions between phthalocyanine compounds containing transition metals (TMPcs) and ferromagnetic surfaces for realizing molecular spintronics. Recently we have reported on the ferromagnetic coupling of central metal ions like manganese [1] and iron [2] with ferromagnetic Co films. In this study, we investigated the molecular orientation and magnetic properties of vanadyl phthalocyanine (VOpc) deposited on a ferromagnetic iron surface by using x-ray absorption spectroscopy (XAS) and x-ray magnetic circular dichroism (XMCD).

Sample preparation was carried out in an ultrahigh vacuum condition. First, a ferromagnetic iron film was prepared by the electron bombardment evaporation on a clean Cu(001) substrate at low temperature ( $T \sim 110$  K). The thickness of the iron film was confirmed by the reflection high-energy electron diffraction oscillations during the evaporation. Subsequently, purified VOpc was deposited on the iron film using a homemade Knudsen cell at 570 K. During the sublimation deposition, the substrate was kept at room temperature. The deposition rate estimated by a quartz crystal oscillator was 0.1 ML/min and the amount of deposition was 0.9 ML (1 ML = 0.5 molecule/nm<sup>2</sup>). XAS and XMCD measurements were performed at 5 K by means of the total electron yield detection mode. In the XMCD measurement, the helicity of the circularly polarized x-rays was fixed positively while the magnetic field was reversed.

Figure 1(a) shows angle dependence of the linearly polarized N K-edge XAS of 0.9 ML VOpc deposited on the iron surface. The peaks labeled A, B and C are mainly attributed to transitions from N 1s to the  $\pi^*$  molecular orbitals and the intensity of the  $\pi^*$  peaks increases with increasing the x-ray incidence angle. This indicates that the framework of phthalocyanine is adsorbed with a flat orientation. In addition, the satellite peak S is observed due to strong interaction of the N atoms with the iron surface.

Figure 1(b) shows V L-edge and O K-edge circularly polarized XAS and XMCD spectra at the incident angle of 0° and 55°. Although the XMCD spectra or the magnetization curves for the iron film were not shown, we confirmed that the magnetization of the iron film is saturated at 5 T in both the 0° and 55° configurations. The XMCD signal is detected at the V L-edge, which means that the V spin in VOpc is maintained. Then, the XMCD signal shows a

positive sign at the V L<sub>3</sub>-edge, while it is negative at the Fe L<sub>3</sub>-edge. This implies that the central vanadium ions are magnetized to the opposite direction to the magnetization of the iron film. In contrast to the previous cases of MnPc/Co and FePc/Co systems, the spins of the central vanadium ions are antiferromagnetically coupled with those of the iron atoms in the ferromagnetic iron film.

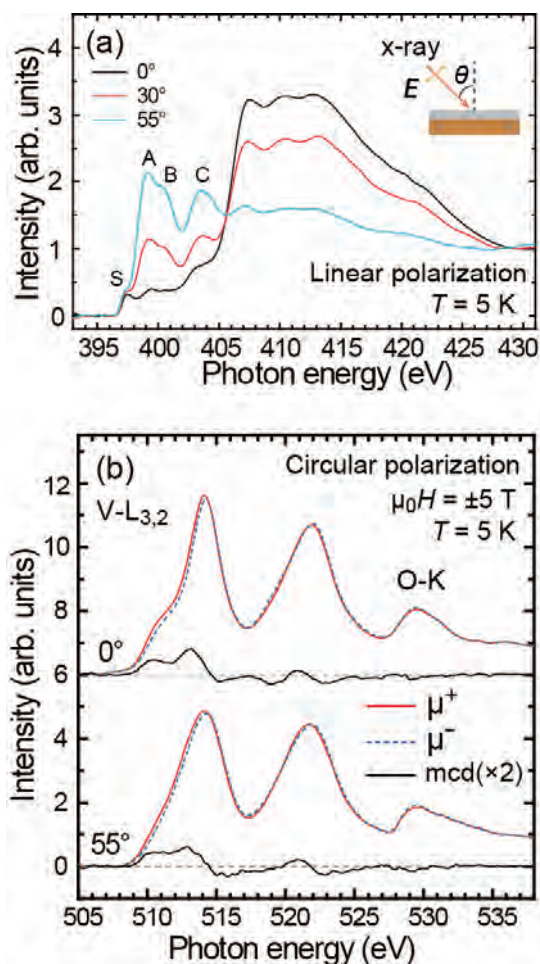


Fig. 1. (a) The linearly polarized N K-edge XAS intensities of 0.9 ML VOpc on Fe (3 ML)/Cu(001). (b) V L-edge and O K-edge XAS and XMCD spectra of 0.9 ML VOpc on Fe (3 ML)/Cu(001) taken at the incident angle of 0° and 55° from the surface normal at  $T=5$  K and  $\mu_0 H=5$  T.

[1] I. Yamamoto *et al.*, UVSOR ACTIVITY REPORT **37** (2010) 74.

[2] Y. Takagi *et al.*, UVSOR ACTIVITY REPORT **38** (2011) 74.

BL5U

## Photoemission Study of $\text{CaCu}_3\text{Ru}_4\text{O}_{12}$

H. J. Im<sup>1</sup>, M. Iwataki<sup>1</sup>, M. Tsunekawa<sup>2</sup>, T. Watanabe<sup>1</sup>, M. Matsunami<sup>3,4</sup> and S. Kimura<sup>3,4,5</sup>

<sup>1</sup>Department of Advanced Physics, Hirosaki University, Hirosaki 036-8224, Japan

<sup>2</sup>Faculty of Education, Shiga University, Hikone 522-8522, Japan

<sup>3</sup>UVSOR Facility, Institute for Molecular Science, Okazaki 444-8585, Japan.

<sup>4</sup>School of Physical Sciences, The Graduate University for Advanced Studies, Okazaki 444-8585, Japan.

<sup>5</sup>Graduate School of Frontier Biosciences, Osaka University, Suita, 565-0871, Japan.

A-site ordered perovskite compounds of the stoichiometry of  $\text{AA}'_3\text{B}_4\text{O}_{12}$  are formed by the substitution of three-fourths of A-site ions by A'-site ions in the typical  $\text{ABO}_3$  structure. Particularly,  $\text{CaCu}_3\text{B}_4\text{O}_{12}$  compounds (B:  $\text{Ti}^{4+}$ ,  $\text{Ru}^{4+}$ ,  $\text{Mn}^{4+}$ ,  $\text{Fe}^{3+}$ ) have been attracted much attention due to a variety of intriguing physical properties which come from the strong correlation effects. For instance,  $\text{CaCu}_3\text{Ti}_4\text{O}_{12}$  (CCTO), which shows extremely high dielectric constant [1], is Mott-insulator which has turned out to be caused by the band shift and the band narrowing in angle-resolved photoemission studies [2, 3]. And  $\text{CaCu}_3\text{Ru}_4\text{O}_{12}$  (CCRO) have extensively studied due to heavy-fermion like behaviors and non-Fermi liquid behaviors [4, 5].

Here, in order to understand the underlying physics of A-site ordered perovskites, we have performed photoemission measurements on CCRO at BL5U and compared it with the previous results of CCTO.

The polycrystalline sample has been synthesized by conventional solid state reaction technique using  $\text{CaCO}_3$ ,  $\text{CuO}$ , and  $\text{TiO}_2$ . In order to decompose the calcium carbonate, stoichiometric mixtures were initially calcined at 700 °C for 12 h. The pressed pellets were annealed at 1050 °C for 24 h. Single phase has confirmed by X-ray diffraction pattern.

The photon energy of 90 eV was used in PES measurements. The clean sample surface was prepared by *in situ* cleaving in the ultra-high vacuum. The measurement temperature is 300 K.

Figure 1 shows the PES spectra of CCRO and CCTO in the valence band regime obtained by angle-integrated analyzer mode. We recognized the spectral shape of CCRO is similar with CCTO except for the Fermi level. The most intensive peaks are observed around 4 eV which come from the mainly Cu 3d states. Interestingly, the peak positions are almost same in CCRO and CCTO. It was already reported in CCTO that the Cu 3d peaks are shifted to higher binding energy due to strong correlation effects, indicating the localized character [2]. In 5 – 8 eV, the broad peak are mainly O 2p states. The hump around 2.5 eV are observed. Particularly, in CCRO the spectral weights are clearly observed near the Fermi-level where there are mainly Ru 4d-states in the band calculations, indicating the itinerant character.

We have reported that most Ti 3d states in CCTO are located in the unoccupied regime [2]. In contrast,

Ru 4d states are expected to be exist in the occupied regime due to strong hybridization of broader Ru 4d states with Cu 3d and O 2p states in the band calculations. Therefore, we suggest that the differences of the spectral shape between CCTO and CCRO are attributed to the participation of Ru 4d states in the occupied regime.

For future work, it should be studied how the itinerant Ru 4d states and the localized Cu 3d states play a role in heavy-fermion behaviors and non-Fermi liquid behaviors.

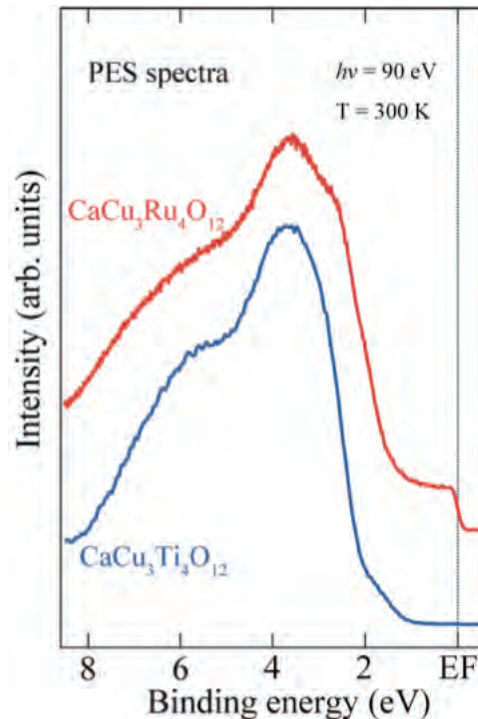


Fig. 1. Photoemission spectra of  $\text{CaCu}_3\text{Ru}_4\text{O}_{12}$  and  $\text{CaCu}_3\text{Ti}_4\text{O}_{12}$  in the valence band regime at room temperature, obtained at  $h\nu = 90$  eV.

- [1] M. A. Subramanian *et al.*, J. Solid State Chem. **151** (2000) 323.
- [2] H. J. Im *et al.*, Phy. Rev. B **88** (2013) 205133.
- [3] H. J. Im *et al.*, UVSOR Activity Report **40** (2013) 100.
- [4] W. Kobayashi *et al.*, J. Phys. Soc. Jpn. **73** (2004) 2373.
- [5] A. Krimmel *et al.*, Phys. Rev. B **78** (2008) 165126.

BL5U

## Soft X-Ray Photoemission Spectroscopy Study of Fe<sub>2</sub>P(0001) and Ni<sub>2</sub>P(0001)

Y. Sugizaki<sup>1</sup>, S. Ishida<sup>1</sup>, T. Nakamura<sup>1</sup> and K. Edamoto<sup>1,2</sup>

<sup>1</sup>Department of Chemistry, Rikkyo University, Tokyo 171-8501, Japan

<sup>2</sup>Research Center for Smart Molecules, Rikkyo University, Tokyo 171-8501, Japan

The transition metal phosphides (TMPs) have attracted much attention because these materials show high catalytic activity for hydrodesulfurization (HDS) and hydrodenitritization (HDN)<sup>[1]</sup>. Of all TMPs, Ni<sub>2</sub>P shows the highest catalytic activity for HDS, while that of Fe<sub>2</sub>P is extremely low<sup>[1]</sup>. The difference is thought to originate from the difference in electric structure of surface metal atoms. The surface electronic structure of Ni<sub>2</sub>P has been investigated by XPS, and it has been proposed that active Ni sites are stabilized through the bonding with segregated P atoms<sup>[2]</sup>. As for Fe<sub>2</sub>P, very little information is available at present. To comprehend the origin of difference in catalytic activities, we investigated surface properties of Ni<sub>2</sub>P(0001) and Fe<sub>2</sub>P(0001) by using soft X-ray photoemission spectroscopy (SXPS).

The experiments were performed at BL-5U of UVSOR, Institute for Molecular Science. The photoelectrons were collected by an electron energy analyzer of hemispherical type (MBS A-1), using an angle-integrated mode (acceptance angle of  $\pm 20^\circ$ ). The Ni<sub>2</sub>P and Fe<sub>2</sub>P single-crystals were grown by Dr. S. Otani of National Institute for Materials Science. The samples were cut at an orientation of (0001) by spark erosion, and the surfaces were polished mechanically to a mirror finish. The clean surfaces were prepared by several cycles of Ar<sup>+</sup> ion sputtering and several temperature annealing (600 ~ 900 K).

Figure 1 shows the P2p core-level spectra of Ni<sub>2</sub>P (a) and Fe<sub>2</sub>P (b) measured at  $h\nu=170\text{eV}$ . The background drawn by a Shirley procedure has been subtracted from each raw data. For Ni<sub>2</sub>P, major peaks ( $2p_{3/2}$  and  $2p_{1/2}$  levels) are observed at 129.6 and 130.4eV, respectively, together with shoulder peaks around 129.9 and 130.7eV. Both shoulder peaks disappear by slight sputtering, and thus the shoulders are associated with segregated P atoms. For Fe<sub>2</sub>P, in addition to the major peaks at 129.3 and 130.1eV, several minor peaks are observed in the region between 129 and 128eV. These peaks disappear by slight sputtering, and thus these are associated with segregated P atoms. These results indicate that P segregation occurs by annealing for both Ni<sub>2</sub>P(0001) and Fe<sub>2</sub>P(0001).

Figure 2 shows valence band spectra of Ni<sub>2</sub>P (a) and Fe<sub>2</sub>P (b). The bands observed at 0-4.5eV for Ni<sub>2</sub>P and at 0-4eV for Fe<sub>2</sub>P are Ni3d-P3p hybrid band and Fe3d-P3p hybrid band, respectively. For Ni<sub>2</sub>P, annealing the sputtered surface at 900K induces the shift of the whole band toward the higher binding

energy side and the growth of a new peak at 3.4eV, which is induced by bonding between Ni and segregated P atoms. These result shows that the surface Ni atoms are stabilized due to a ligand effect. On the other hand, valence band spectra of Fe<sub>2</sub>P shows little change by annealing the sputtered surface, indicating that the ligand effect is not effective on Fe<sub>2</sub>P(0001). These results suggest that the control of the electronic structure of active metal sites is important to improve the catalytic performance of TMPs.

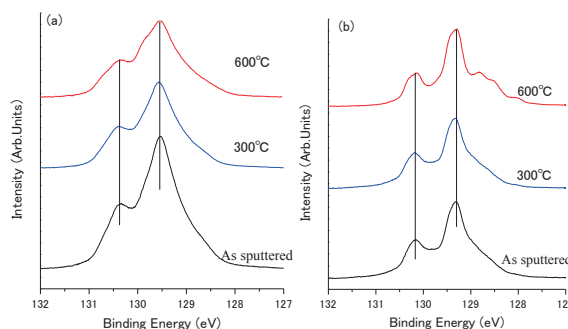


Fig. 1. P2p core-level spectra ( $h\nu=170\text{eV}$ ) for (a) Ni<sub>2</sub>P(0001) and (b) Fe<sub>2</sub>P(0001).

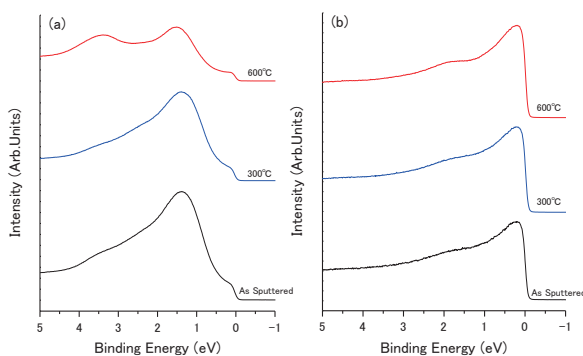


Fig. 2. Valence band spectra of Ni<sub>2</sub>P (a) and Fe<sub>2</sub>P (b). Ni<sub>2</sub>P was measured at  $h\nu=60\text{eV}$  and Fe<sub>2</sub>P was measured at  $h\nu=49\text{eV}$ .

[1] S. T. Oyama, *J. Catal.* **216** (2003) 343.

[2] K. Edamoto, *et al.*, *Solid. Statate. Communication.* **148** (2008) 135.

[3] Y. Sugizaki, *et al.*, *Surf. Sci.* **624** (2014) 21.

BL5U

## Electronic Structure of a Magnetic Insulator / Topological Insulator Thin Film Heterostructure: MnSe / Bi<sub>2</sub>Se<sub>3</sub>

T. Hirahara<sup>1</sup>, T. Kubo<sup>1</sup>, T. Nakamura<sup>1</sup>, T. Hajiri<sup>2</sup>,  
M. Matsunami<sup>2</sup>, S. Kimura<sup>2</sup> and S. Hasegawa<sup>1</sup>

<sup>1</sup>Department of Physics, University of Tokyo, Tokyo 113-0033, Japan

<sup>2</sup>UVSOR Facility, Institute for Molecular Science, Okazaki 444-8585, Japan

The metallic surface states of three-dimensional topological insulators are protected by time reversal symmetry (TRS). Although breaking TRS is generally detrimental to these states, it may also lead to exotic topological quantum effects, such as magnetic monopoles, quantized anomalous Hall effect, and giant magneto-optical effects. In terms of electronic structure, it has been predicted that the massless Dirac-cone (DC) surface states will undergo gap opening and become massive [1].

Up to now, most studies that have tried to break TRS in topological insulators have been performed with magnetic impurity doping in the bulk or at the surface [2]. Although this is a straightforward and simple strategy, various results have been reported that are in favor/unfavor of the TRS breaking in terms of gap-opening of the DC [3]. One study has even shown that a gap-opening is observed even when nonmagnetic impurities are incorporated [4]. Therefore, an alternative method to induce TRS breaking in topological insulators with well-defined structures is called for.

In the present study, we have fabricated a heterostructure of thin films of magnetic (MnSe) and topological insulators (Bi<sub>2</sub>Se<sub>3</sub>) and tried to see whether a gap opening can be observed in the DC. These two materials have nearly the same lattice constant and can be made into a heterostructure as confirmed with diffraction measurements. Although MnSe is an antiferromagnetic insulator, theoretical calculation predicts that a magnetic interaction at the interface is expected to induce a gap opening in the DC [5]. Figure 1 shows the band dispersion of a 10 quintuple layer (QL) Bi<sub>2</sub>Se<sub>3</sub> film (a) and a heterostructure of 2.4 bilayer (BL) MnSe / 10 QL Bi<sub>2</sub>Se<sub>3</sub> film (b). One can notice that the DC remains after MnSe deposition although its intensity has decreased drastically. Furthermore, the Dirac point has shifted towards the Fermi level, making the bulk insulating. The origin of this shift is unclear at the moment. Moreover, whether a gap has opened at the Dirac point is also not clear and needs higher resolution measurements.

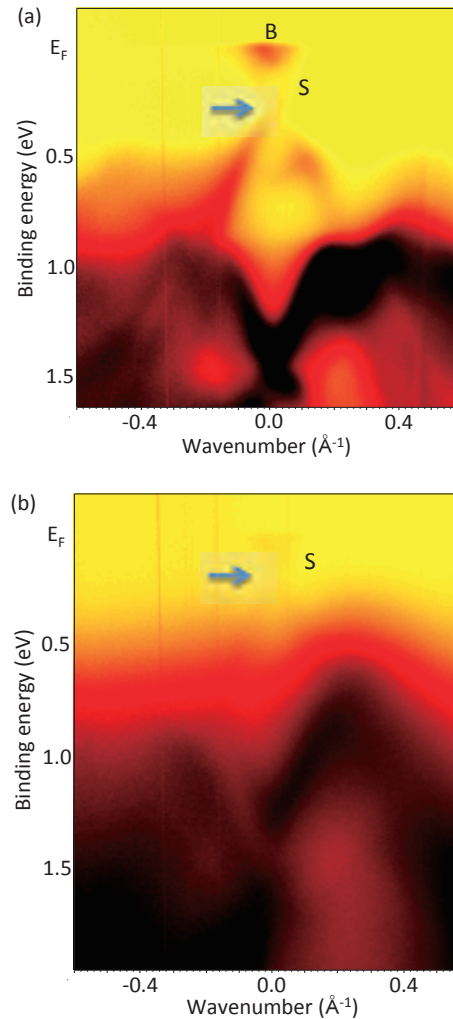


Fig. 1. Band dispersion of a 10 quintuple layer (QL) Bi<sub>2</sub>Se<sub>3</sub> film, (a) and a heterostructure of 2.4 bilayer (BL) MnSe / 10 QL Bi<sub>2</sub>Se<sub>3</sub> film, (b). S and B correspond to surface and bulk states and the arrows indicate the Dirac point.

- [1] M. Z. Hasan and C. L. Kane, *Rev. Mod. Phys.* **82** (2010) 3045.
- [2] S.-X. Xu *et al.*, *Nat. Phys.* **8** (2012) 616.
- [3] A. Varykhalv *et al.*, *Phys. Rev. X* **2** (2012) 041017.
- [4] T. Sato *et al.*, *Nature Physics* **7** (2011) 840.
- [5] S. V. Eremeev *et al.*, *Phys. Rev. B* **88** (2012) 144430.

BL5U

## Angle-Resolved Photoemission Study of $\text{Ba}_3\text{Co}_2\text{O}_6(\text{CO}_3)_{0.7}$

T. Hosokawa<sup>1</sup>, T. Hajiri<sup>1,2</sup>, T. Ito<sup>1,3</sup>, M. Matsunami<sup>2,4</sup>, S. Kimura<sup>2,5</sup>,  
Y. Shimizu<sup>6</sup>, Y. Kobayashi<sup>6</sup> and M. Ito<sup>6</sup>

<sup>1</sup>Graduate School of Engineering, Nagoya University, Nagoya 464-0818, Japan

<sup>2</sup>UVSOR Facility, Institute for Molecular Science, Okazaki 444-8585, Japan

<sup>3</sup>Nagoya University Synchrotron Radiation Research Center, Nagoya University, Nagoya 464-8603, Japan

<sup>4</sup>School of Physical Sciences, The Graduate University for Advanced Studies (SOKENDAI), Okazaki 444-8585, Japan

<sup>5</sup>Graduate School of Frontier Biosciences and Physics Department, Osaka University, Osaka 565-0871, Japan

<sup>6</sup>Graduate School of Science, Nagoya University, Nagoya 464-8603, Japan

Cobalt oxides have attracted attention due to their anomalous electronic/magnetic properties such as a large thermoelectric power. Recently it has been found that a quasi-one-dimensional cobaltate  $\text{Ba}_3\text{Co}_2\text{O}_6(\text{CO}_3)_{0.7}$  shows a fairly large thermoelectric power comparable to one of  $\text{Na}_0.75\text{CoO}_2$ . In order to understand its physical properties, we have investigated the electronic structure of  $\text{Ba}_3\text{Co}_2\text{O}_6(\text{CO}_3)_{0.7}$  by utilizing angle-resolved photoemission spectroscopy (ARPES).

ARPES measurements were performed at the beamline BL5U of UVSOR-III. Clean surfaces were obtained by *in situ* cleaving the samples in perpendicular to the *c* axis.

Figure 1 shows the ARPES image near the Fermi level ( $E_F$ ) along the  $\Gamma A$  high-symmetry line measured at  $T = 20$  K. We successfully obtain the clear dispersive features from 0.5 to 3 eV binding energy range. From the comparison with the Co 3p-3d resonant photoemission result of  $\text{Ba}_3\text{Co}_2\text{O}_6(\text{CO}_3)_{0.7}$ , the observed bands mainly consist of the Co 3d orbital character [3]. To show the symmetry of the electronic structure clearly, we have mapped out the intensity of ARPES spectra around 0.5 eV (valence band maximum) in the  $\Gamma A$ - $\Gamma KM$  plane as indicated in Fig. 2. From the constant energy intensity map, we can find that the line-shape contrast along the AHL high-symmetry line. Furthermore, the intensity increases from the A to L point. It is expected that the one-dimensional atomic (molecular) chain form the plate-like electronic structure perpendicular to the one-dimensional conducting axis. Thus, the observed symmetry of the ARPES intensity ensures the appropriate sample setup along the quasi-one dimensional face-sharing CoO6 chains.

In contrast to the metallic/semimetallic properties on electronic conductivity along *c* axis, the valence band maximum seems to be located around 0.5 eV in Fig. 1. It should be noted that the ARPES spectra exhibit a low energy tail from 0.5 eV to  $E_F$  around the A point, though the tail feature does not cross  $E_F$ . To understand the origin of this discrepancy, more detailed ARPES measurements are intended.

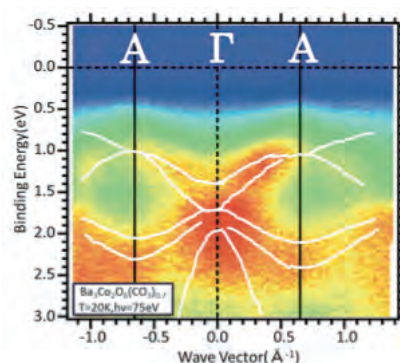


Fig. 1. ARPES image of  $\text{Ba}_3\text{Co}_2\text{O}_6(\text{CO}_3)_{0.7}$  along the  $\Gamma A$  high-symmetry line measured at  $T=20$ K. White lines are guide for eyes to trace a main dispersive feature.

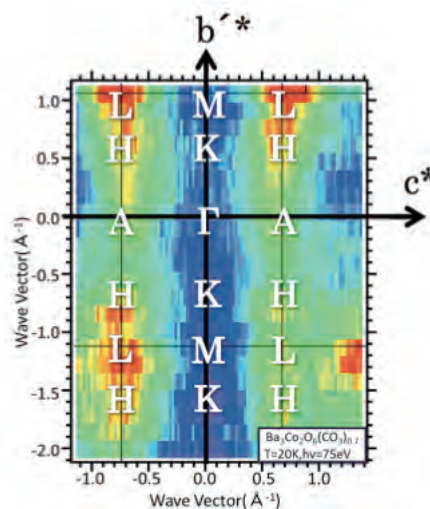


Fig. 2. The Valence Band Maximum ( $E_B=0.5\text{eV}$ ) surface in the  $\Gamma A$ - $\Gamma KM$  plane of  $\text{Ba}_3\text{Co}_2\text{O}_6(\text{CO}_3)_{0.7}$  mapped by ARPES at  $T=20$ K.

[1]K. Iwasaki *et al.*, JOURNAL OF APPLIED PHYSICS **106** (2009) 034905.

[2]K. Igarashi *et al.*, Journal of Physics: Conference Series **400** (2012) 032024.

[3]K. Soda *et al.*, UVSOR Activity Report **37** (2010) 99.

BL5B

## Photoinduced Changes of Amorphous Chalcogenide Thin Films Studied by Vacuum Ultraviolet Transmission Spectroscopy

K. Hayashi

*Department of Electrical, Electronic and Computer Engineering, Gifu University, Gifu 501-1193, Japan*

It is well-known that amorphous chalcogenide semiconductor materials show a variety of photoinduced effects [1-3] and are very expected as a potential material for optoelectronic devices because these materials are very sensitive to the light. For the device application, it is necessary to sufficiently understand the physical property of these materials. Although a large number of studies have been done on the photoinduced phenomena of these materials, little is known about the details of these mechanisms. These phenomena were studied by exciting outer core electrons with the irradiation of light with the energy corresponding to the optical bandgap or sub-bandgap. The interest has been attracted for the change of the optical properties in the energy region of the visible light. We are interesting for the changes of the optical properties in the higher energy region. To obtain a wide knowledge of the photoinduced phenomena, it is necessary to investigate to the photoinduced effects on wide energy region. Recently, we became able to measure directly the VUV transmission spectra of amorphous thin films [4]. In this paper we report on the study of the photoinduced changes of the as-deposited amorphous chalcogenide thin films before and after irradiation of the bandgap (BG) light by the VUV transmission spectroscopy.

Samples used for the measurement of the VUV transmission spectrum were amorphous chalcogenide (a-As<sub>2</sub>Se<sub>3</sub> and a-As<sub>2</sub>S<sub>3</sub>) semiconductor thin films prepared onto aluminum thin films by conventional evaporation technique. Typical thickness of the samples and the aluminum films were around 180nm and 200nm respectively. The aluminum film was also used in order to eliminate the higher order light from the monochromator in the VUV region. The measurements were carried out at room temperature at the BL5B beam line of the UVSOR facility of the Institute for Molecular Science. And the spectrum was measured by using the silicon photodiode as a detector. A pinhole of 1.5mm in a diameter was inserted between the monochromator and sample to remove stray light. The intensity of the VUV light was monitored by measuring the TPEY of a gold mesh. The positions of the core levels for the samples were calibrated by referencing to the 2p core level absorption peak of the aluminum film.

Figure 1 shows the VUV transmission spectra of the 3d core levels of Se and As atoms in a-As<sub>2</sub>Se<sub>3</sub> film before and after the irradiation of the BG light. As shown in the figure, the photoinduced changes are observed on the transmission spectra before and after

the irradiation of the BG light.

Those changes might relate to the photoinduced defects created by the irradiation of the BG light. More detailed experiments are necessary to clarify the origin of the photoinduced changes of the VUV transmission spectra.

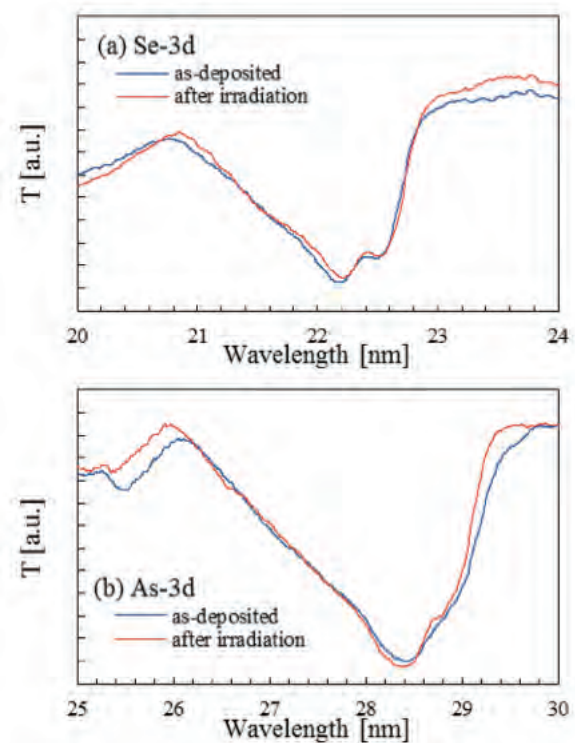


Fig. 1. VUV transmission spectra of (a) Se 3d and (b) As 3d core levels of as-deposited a-As<sub>2</sub>Se<sub>3</sub> thin film before and after the irradiation of the BG light.

- [1] K. Tanaka, *Rev. Solid State Sci.* **4** (1990) 641.
- [2] K. Shimakawa, A. Kolobov and S. R. Elliott, *Adv. Phys.*, **44** (1995) 475.
- [3] K. Tanaka, *Encyclopedia of Nanoscience and Nanotechnology*, **7** (2004) 629.
- [4] K. Hayashi, *UVSOR Activity Report* **34** (2007) 79.

BL6U

## Hydrogen Interaction on MoS<sub>2</sub> Surface

 S. W. Han<sup>1,2</sup>, H. Yamane<sup>3</sup>, N. Kosugi<sup>3</sup> and H. W. Yeom<sup>1,2</sup>
<sup>1</sup>Center for Artificial Low Dimensional Electronic Systems, Institute for Basic Science (IBS), 77 Cheongam-Ro, Pohang 790-784, Korea

<sup>2</sup>Department of Physics, Pohang University of Science and Technology, 77 Cheongam-Ro, Pohang 790-784, Korea

<sup>3</sup>Institute for Molecular Science, Myodaiji, Okazaki 444-8585, Japan

Recently, it has been reported that the hydrogenated MoS<sub>2</sub> induced a weak ferromagnetism persisting up to room temperature (RT) with the improved transport property [1]. It is important to understand the interaction between the H<sub>2</sub> molecule and the MoS<sub>2</sub> surface.

Angle-resolved photoemission (ARPES) experiments were performed at the undulator beamline BL6U of UVSOR-III in the Institute for Molecular Science. Natural and single crystalline MoS<sub>2</sub> samples were cleaved in UHV. The orientation of samples was confirmed by a hexagonal pattern in low-energy electron diffraction and the band structure from the ARPES data, which were collected at 140 K in the main chamber with a base pressure of  $1 \times 10^{-10}$  torr. The total energy and angular resolutions of the ARPES apparatus were better than 25 meV and  $0.1^\circ$ . The MoS<sub>2</sub> surface was exposed to the H<sub>2</sub> gas at RT by back filling the chamber with a pressure of  $1 \times 10^{-6}$  torr and postannealed in the preparation chamber.

Figure 1(a) shows the ARPES data of a cleaved MoS<sub>2</sub> surface along the  $\Gamma$ -K high-symmetry line of the hexagonal Brillouin zone. ARPES data were recorded with a photon energy of 100 eV and scaled by the maximum intensity. A valence band maximum (VBM) is located at the  $\Gamma$ -point with a binding energy of 0.34 eV. Below the VBM at  $\Gamma$ , there exists a strong band dispersing down (red rectangle) from the binding energy of 0.60 eV. This state is known to be a surface state, with the main contribution from the S 3p<sub>z</sub> orbital on the top S layer above the Mo layer within a topmost layer of bulk MoS<sub>2</sub>, while the VBM originates mainly from the Mo 4d<sub>z<sup>2</sup></sub> orbital [2]. On the other hand, the top of the valence band dispersion at the K point ( $1.325 \text{ \AA}^{-1}$ , vertical dashed lines), stems from the mixed states of Mo 4d<sub>xy/x<sup>2</sup>-y<sup>2</sup></sub> and S 3p<sub>xy</sub> orbitals and is located at a higher binding energy of 0.80 eV than that of VBM. This confirms the indirect bandgap of bulk MoS<sub>2</sub>.

Figure 1(b) exhibits the band structure of MoS<sub>2</sub> surface after an exposure to hydrogen gas for 600 s, corresponding to 600 L ( $1 \text{ L} = 10^{-6} \text{ Torr}\cdot\text{s}$ ). Despite of the hydrogen exposure, band structure remains unchanged. Instead, the VBM slightly shifted toward Fermi energy ( $E_F$ ) and it is located at 0.26 eV with a quite obvious band dispersion. The VBM further shifts to 0.20 eV in the case of a longer exposure of a new MoS<sub>2</sub> surface to the H<sub>2</sub> gas for 3600 s (3600 L)

as shown in Fig. 1(c).

In contrast, after postannealing at 300 °C for 1 h [Fig. 1(d)], the VBM is located at the binding energy of 0.75 eV, which reversely shifted away from  $E_F$ .

In order to elucidate the hydrogenation, another MoS<sub>2</sub> sample was cleaved and annealed at 300 °C and then exposed to the H<sub>2</sub> gas for 1.5 h (5400 L). In Fig. 1(e), the VBM is obtained at a much higher binding energy of 1.24 eV with slightly broadened spectral features. Especially S p<sub>z</sub> derived bands are enhanced at the higher binding energy side.

Figure 1(f) represents the shift of valence-band spectra, which were integrated from the ARPES data and normalized by the intensity of the first peak indicated by the (red) lines. Without a significant change of band structure, the H<sub>2</sub> exposure leads to shift the VBM toward  $E_F$  while the annealing shifts the VBM away from  $E_F$ .

These results suggest that the thermal annealing promotes the dissociation of H<sub>2</sub> molecules on the MoS<sub>2</sub> surface and then the atomic hydrogens are intercalated between van der Waals gaps.

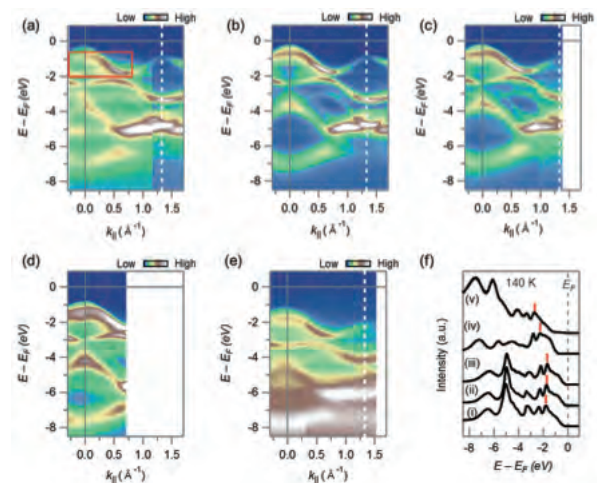


Fig. 1. ARPES intensity maps along the  $\Gamma$ -K direction of the Brillouin zone for three MoS<sub>2</sub> samples.

[1] S. W. Han *et al.*, Phys. Rev. Lett. **110** (2013) 247201.

[2] S. W. Han *et al.*, Phys. Rev. B. **86** (2012) 115105.

BL6U

## Electronic Structure of Epitaxial, Metallic Germanium Nanofilms on Zirconium Diboride Thin Film Substrates – Identification of a New Form of Crystalline Germanium

R. Friedlein<sup>1</sup>, H. Yamane<sup>2</sup>, N. Kosugi<sup>2</sup> and Y. Yamada-Takamura<sup>1</sup>

<sup>1</sup>*School of Materials Science, Japan Advanced Institute of Science and Technology, Nomi 923-1292, Japan*

<sup>2</sup>*Dept. of Photo-Molecular Science, Institute for Molecular Science, Okazaki 444-8585, Japan*

While Si and Ge are right below C in the periodic table of elements, valence orbitals of Si and Ge atoms do not  $sp^2$  hybridize as easily as for their smaller counterpart. However, considering that the experimental evidence for the existence of the largely  $sp^2$ -hybridized form of silicon called “epitaxial silicene” mounting [1-3], the verification of layered, hexagonal germanium structures with Dirac-cone like electronic signatures – in analogy to graphene and silicene conveniently coined “germanene” – would represent another important step towards novel two-dimensional nano-materials.

In this context, recently, in our home laboratory, we have succeeded in the preparation of nanofilms of germanium on the surface of  $ZrB_2(0001)$  thin films grown on Ge(111) wafers. These epitaxial, single-crystalline-like Ge nanofilms are formed by surface segregation at elevated temperatures and oxidize upon exposure to air.

However, the native oxide can be removed by an annealing procedure under ultra-high vacuum conditions upon which again Ge nanofilms are formed. At BL6U, these films have then been studied *in situ* by angle-resolved valence band (ARPES) and core-level (XPS) photoelectron spectroscopy as well as by low-energy electron diffraction (LEED).

The measured electronic and structural properties of the films are consistent with a layered structure of hexagonal symmetry and a  $(1 \times 1)$  in-plane lattice constant that is about 20 % smaller than that of bulk germanium in the diamond crystal structure.

Figure 1 shows the valence band structure along the  $\bar{\Gamma}$ - $\bar{K}$  direction of the  $(1 \times 1)$  diboride Brillouin zone, as obtained at 15 K. A manifold of well-defined states with upwards curvature are observed. These states are likely thin film slab states that are related to the layered structure of the nanofilms. Some of these states cross the Fermi level indicating that the films are metallic. This behavior is expected for highly-strained germanium layers in which  $\sigma$  states are partially pushed above  $E_F$  [4].

At room temperature, the films are  $(\sqrt{3} \times \sqrt{3})$ -reconstructed; on the other hand, below about 100 K, the films undergo a phase transition into a  $3\sqrt{3} \times 3\sqrt{3}$  structure. This phase transition is connected to a significant change in the low-energy band structure which may be associated with a charge-density wave ground state related to an electronic instability

characteristic of low-dimensional systems. This may indicate that the interlayer coupling is weaker than anticipated.

At present, the results are compared with those of quantum-chemical calculations in order to understand both the structural and electronic properties.

This work was supported by the Joint Studies Program (No. 615, 2012~2013) of the Institute for Molecular Science.

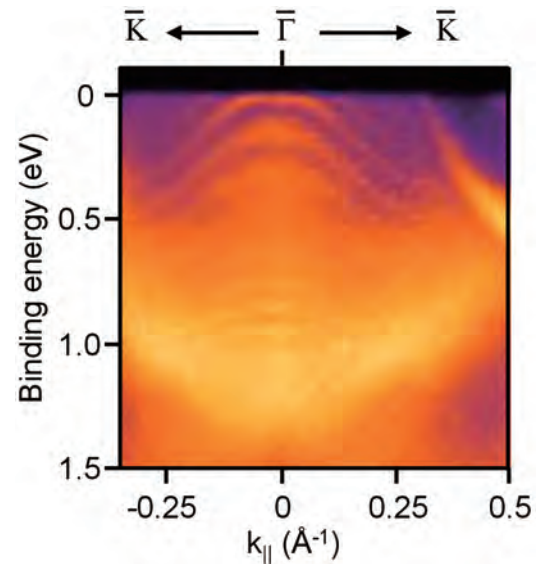


Fig. 1. ARPES spectrum of a Ge nanofilm on  $ZrB_2(0001)$  thin films on Ge wafers, along the  $\bar{\Gamma}$ - $\bar{K}$  direction, with the sample held at 15 K. The photon energy of 43 eV was used.

[1] P. Vogt, P. De Padova, C. Quaresima, J. Avila, E. Frantzeskakis, M. C. Asensio, A. Resta, B. Ealet and G. Le Lay, *Phys. Rev. Lett.* **108** (2012) 155501.

[2] A. Fleurence, R. Friedlein, T. Ozaki, H. Kawai, Y. Wang and Y. Yamada-Takamura, *Phys. Rev. Lett.* **108** (2012) 245501.

[3] R. Friedlein, A. Fleurence, J. T. Sadowski and Y. Yamada-Takamura, *Appl. Phys. Lett.* **102** (2013) 221603.

[4] Y. Wang and Y. Ding, *Solid State Commun.* **155** (2013) 6.

BL6U

## Formation of Interface State and Intermolecular Band Dispersion in Coronene/Au(111) Superstructure

H. Yamane and N. Kosugi

Department of Photo-Molecular Science, Institute for Molecular Science, Okazaki 444-8585, Japan

Study of organic/metal interfaces is essential to investigate electronic phenomena derived from the complex interplay between van der Waals interaction and exchange-correlation interaction. Previous studies on organic/metal energetics have been performed mainly for non-ordered or multi-domain systems due to experimental difficulties. In the present work, we applied the precise angle-resolved photoemission spectroscopy (ARPES) to the single-domain monolayer of coronene physisorbed on Au(111).

The present experiments were performed at BL6U. The cleanliness of the Au(111) surface was confirmed by the low-energy electron diffraction with a micro channel plate (MCP-LEED) and the Shockley surface state in ARPES, as obtained from the repeated cycles of the Ar<sup>+</sup> sputtering ( $I \sim 2 \mu\text{A}$ ) and the subsequent annealing ( $T = 700 \text{K}$ ). The total energy resolution in the present ARPES measurement was 16 meV.

Figure 1 shows (a) the LEED image and (b) the surface Brillouin zone (SBZ) of the coronene monolayer deposited on Au(111). The LEED image shows the (4×4) single-domain superstructure with respect to the Au(111) hexagonal surface lattice.

The energy-*vs*-momentum  $E(\mathbf{k})$  map along the  $\bar{\Gamma}$ - $\bar{K}$  direction ( $\mathbf{k}_{\text{TK}}$ ) of the clean Au(111) surface and the coronene/Au(111) interface, obtained from ARPES, is shown in Figs. 2(a) and 2(b), respectively. Upon the formation of the coronene/Au(111) superstructure, some new electronic states are observed. The free-electron-like dispersive bands are weakly appeared below the Fermi level  $E_F$  ( $E_b = 0 \sim 0.4 \text{eV}$ ) and above the Au 5d band ( $E_b = 1.7 \sim 2.4 \text{eV}$ ). The inflection point of the parabolic dispersions appears at the  $\bar{\Gamma}$  point of the monolayer's SBZ ( $\mathbf{k}_{\text{TK}} = 1.08 \text{\AA}^{-1}$ ). The parabolic dispersions at the low- and high- $E_b$  side may originate from the Shockley- and Tamm-type interface states, respectively, both of which are induced by the surface potential due to the coronene superstructure. Here, the  $E_b$  position of the parabolic dispersions are almost the same for the original Shockley and Tamm surface states of the clean Au(111) surface. Therefore, the interface interaction between coronene and Au(111) is considered to be quite weak.

At  $E_b \sim 1.6 \text{eV}$ , a highest occupied molecular orbital (HOMO) peak is observed. The energy distribution curve at  $\mathbf{k}_{\text{TK}} = 1.40 \text{\AA}^{-1}$  shows a sharp HOMO line shape with the high- $E_b$  satellite due to the hole- vibration coupling. This observation also suggests the weak physisorption between coronene and Au(111). Note that, the HOMO peak shows a quite weak but non-negligible dispersion of  $\sim 20 \text{meV}$ .

The in-plane band dispersion of molecular electronic states has been observed for strongly chemisorbed interfaces with larger dispersion of 0.2~0.3 eV due to the interfacial orbital hybridization [1, 2]. By considering the quite weak interaction between coronene and Au(111), the observed in-plane band dispersion is ascribed to the genuine intermolecular interaction in two-dimensional sheets of aromatic hydrocarbons.

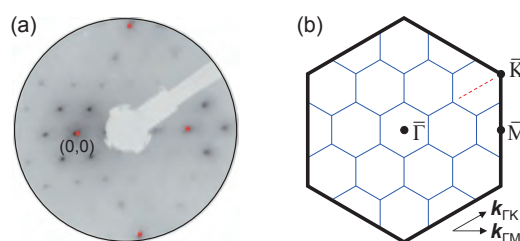


Fig. 1. (a) The MCP-LEED image of the coronene monolayer on Au(111) at 15 K, taken with the 70-eV incident electron beam. The red spot indicates the substrate's spot. (b) The surface Brillouin zone (SBZ) of the monolayer superstructure of coronene on Au(111). The black and blue solid lines indicate the substrate and monolayer SBZs, respectively. The red dashed line indicates the scan region of ARPES.

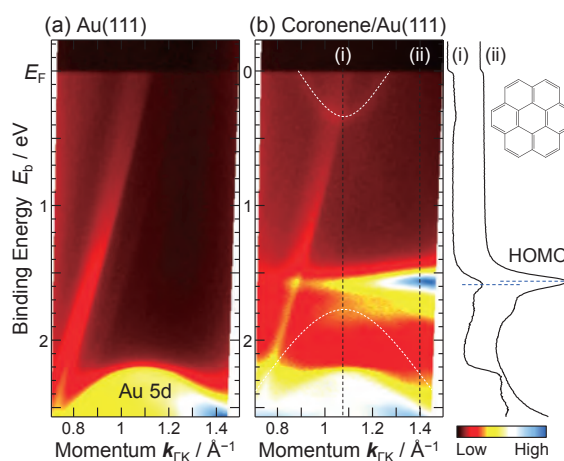


Fig. 2. The  $E(\mathbf{k})$  map at  $T = 15 \text{K}$  around the 2<sup>nd</sup>  $\bar{\Gamma}$  point in the monolayer's SBZ [cf. Fig. 1(b)]; (a) The clean Au(111) surface. (b) The coronene monolayer on Au(111) with the energy distribution curve at (i)  $\mathbf{k}_{\text{TK}} = 1.08 \text{\AA}^{-1}$  and (ii)  $\mathbf{k}_{\text{TK}} = 1.40 \text{\AA}^{-1}$ . The molecular structure of coronene is also shown.

- [1] H. Yamane *et al.*, Phys. Rev. B **76** (2007) 165436.  
 [2] M. Wießner *et al.*, Nat. Commun. **4** (2013) 1514.

BL6U

## Linearly-Dispersive Electronic States at the Interface of Organic Monolayers on Graphite

H. Yamane and N. Kosugi

Department of Photo-Molecular Science, Institute for Molecular Science, Okazaki 444-8585, Japan

Organic monolayers on solid surfaces show various electronic states and complex electronic phenomena, depending on electronic interactions at their interface. Some interfacial electronic phenomena, such as the charge transfer, have been applied to the control of interface energetics in functional molecular systems. In this work, by using angle-resolved photoemission spectroscopy (ARPES), we succeeded in observation of a linearly-dispersive electronic state at the interface of organic monolayers on graphite.

This work was performed at BL6U. The single-crystalline graphite [Gr(0001)] was obtained by the direct resistive heating of a 6H-SiC(0001) wafer at 1500°C [1], as confirmed by the low-energy electron diffraction (LEED) and the valence band dispersion. In order to obtain the well-ordered organic monolayer, the Gr(0001) substrate was heated at ~120°C during the deposition at 1~2 Å/min. The energy resolution in the present ARPES was 16 meV at 15 K.

Figure 1(a) shows the LEED image of the metal-free phthalocyanine ( $H_2Pc$ ) monolayer on Gr(0001) at 15 K. The observed LEED image indicates the well-known multi-domain structure for Pc molecules on six-fold symmetric surfaces. The molecular unit cell of  $H_2Pc/Gr(0001)$  determined from LEED [Fig. 1(b)] agrees with the previous STM study [2]. Considering the symmetry of the molecular unit cell, we measured the azimuthal-angle-dependent ARPES.

Figure 1(c) shows the energy-*vs*-momentum  $E(k)$  map and its energy- and momentum-distribution curves (EDC and MDC) for  $H_2Pc/Gr(0001)$  at 15 K along the  $b_1^*$  direction ( $h\nu = 45$  eV). The highest occupied molecular orbital (HOMO) peak appears at the binding energy ( $E_b$ ) of 1.4 eV. In addition, as indicated by the dashed line in the  $E(k)$  map and MDC, the linearly-dispersive feature appears weakly but undoubtedly at  $E_b = 0\sim 2.2$  eV, like Dirac cone. This is the interface-specific electronic state, which is observable for neither the clean Gr(0001) surface nor the thick multilayer film. In general, the Dirac cone in a honeycomb structure, such as graphene, is appeared not at the edge but at the corner of the Brillouin zone. In the present case, we found that the linearly-dispersive interface state appears at all azimuth directions. Therefore, the observed linearly-dispersive interface state could be due to the scattering from the Dirac band of the underlying Gr(0001) substrate.

In order to elucidate the origin of the linearly-dispersive interface state, we measured ARPES as functions of temperature, substrate, and molecule. We found that the linearly-dispersive interface state is getting weak at 300 K, and is not observable for the

$H_2Pc/Au(111)$  interface. These results suggest the importance of the electronic coupling between organic monolayers and Gr(0001). Furthermore, the linearly-dispersive interface state is observed also for other monolayers of pentacene, coronene, and  $C_{60}$  grown on highly oriented pyrolytic graphite (HOPG) with different dispersion parameters such as the Fermi momentum ( $k_F$ ) and the Fermi velocity ( $v_F$ ). On the other hand, both  $k_F$  and  $v_F$  at the CoPc/HOPG interface are almost the same as those at the  $H_2Pc/HOPG$  interface, suggesting the importance of the molecular unit cell.

Judging from the present observations, the linearly-dispersive interface state is governed by both the size of the molecular unit cell and the electronic coupling at molecule/graphite interfaces. The Dirac band of the graphite surface could be scattered and modified by the intermolecular phonons of adsorbate's lattices as a result of the surface Umklapp process, which plays a crucial role in the charge/spin extraction in molecule-graphene hybrid systems.

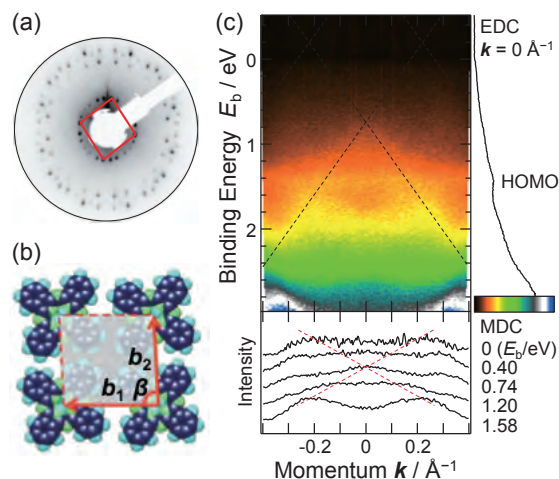


Fig. 1. (a) The LEED image of the  $H_2Pc$  monolayer on Gr(0001) at 15 K, taken with 20-eV incident electrons. (b) The molecular unit cell of  $H_2Pc/Gr(0001)$ , where  $b_1 = 13.8$  Å,  $b_2 = 13.1$  Å, and  $\beta = 87.6^\circ$  [2]. (c) The  $E(k)$  map along the  $b_1^*$  direction with the energy- and momentum-distribution curves (EDC and MDC) of  $H_2Pc/Gr(0001)$  at 15 K ( $h\nu = 45$  eV).

[1] I. Forbeaux *et al.*, Phys. Rev. B **58** (1998) 16396, and references therein.

[2] K. Nilson *et al.*, J. Chem. Phys. **127** (2007) 114702.

BL7U

## Low-Energy Angle-Resolved Photoemission Study on Ultrathin Bi Films II

 T. Hirahara<sup>1</sup>, T. Shirai<sup>1</sup>, M. Matsunami<sup>2</sup>, T. Hajiri<sup>2</sup>, S. Kimura<sup>2</sup> and S. Hasegawa<sup>1</sup>
<sup>1</sup>Department of Physics, University of Tokyo, Tokyo 113-0033, Japan

<sup>2</sup>UVSOR Facility, Institute for Molecular Science, Okazaki 444-8585, Japan

Semimetal bismuth (Bi) is one of the most extensively studied elements in solid state physics because of its extreme physical properties, such as the highest resistivity and Hall coefficient of all metals. Bi has tiny hole and electron pockets at  $T$  and  $L$  points, respectively, [Fig. 1(a) and 1(b)], and therefore the Fermi wavelength  $\lambda_F$  is very large (about 30 nm). Because of this large  $\lambda_F$ , the quantum size effect shows up in the properties of Bi films, and the oscillation of the film resistance with the film thickness  $d$  was reported [1]. Furthermore, it was predicted that when the lowest quantized subband of the electron pocket is raised to an energy higher than the highest hole subband, a band gap will develop [semimetal-to-semiconductor (SMSC) transition at  $d \sim 30$  nm, Fig. 1(c)][2]. However, although many angle-resolved photoemission (ARPES) measurements have been performed on ultrathin Bi films, none has actually been able to verify whether this SMSC transition occurs or not [6-9]. The main reason is that the cross section for the bulk bands depends dramatically on the photon energy and polarization.

Therefore in the present study, we have performed ARPES measurements on ultrathin Bi films by systematically changing the photon energy (7-40 eV) and polarization ( $P$ - and  $S$ - polarization). Figures 2(a) and (b) show the Fermi surface and band dispersion near the Fermi level ( $h\nu = 9.5$  eV) of a 25 Å thick Bi(111) film measured with  $S$ -polarized photons. There is a circular structure at the  $\Gamma$  point. However

when the polarization is switched to  $P$ -polarization ((c) and (d)), it becomes hexagonal. These features correspond to the bulk (B) and surface (S) states, respectively. This suggests that the bulk bands remain metallic and the SMSC transition does not occur. Further sophisticated study is needed to reach a definite conclusion.

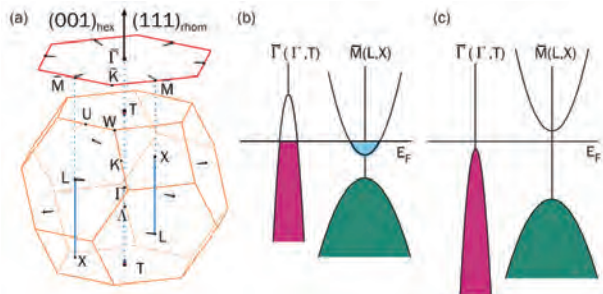


Fig. 1. (a) The Fermi surface of bulk Bi depicted in bulk (orange) and its projection to the surface (red) Brillouin zone. Electron (hole) pockets are filled with light blue (purple). (b), (c) Schematic drawing of the Bi bulk band projection near the Fermi level before (b) and after (c) the SMSC transition [2].

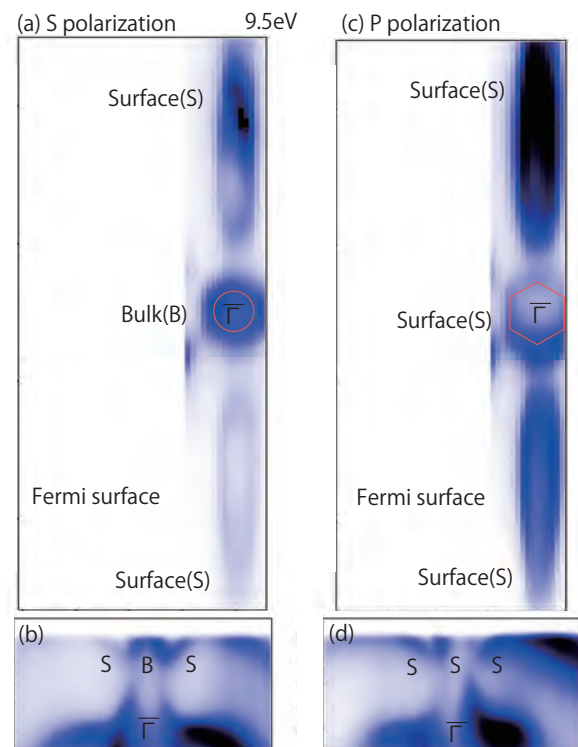


Fig. 2. The Fermi surface and band dispersion of a 25 Å thick Bi(111) film measured at  $h\nu=9.5$  eV with  $S$ - (a), (b) and  $P$ - (c), (d) polarized photons, respectively. S (B) represents surface (bulk) states.

- [1] Yu. F. Ogrin *et al.*, JETP Lett. **3** (1966) 71.
- [2] V. B. Sandomirskii, Sov. Phys. JETP **25** (1967) 101.
- [3] T. Hirahara *et al.*, Phys. Rev. Lett. **97** (2006) 146803; Phys. Rev. B **75** (2007) 035422; Phys. Rev. B **76** (2007) 153305; New Jour. Phys. **10** (2008) 083038.
- [4] A. Takayama *et al.*, Phys. Rev. Lett. **106** (2011) 166401; Nano Lett. **12** (2012) 1766.
- [5] H. Miyahara *et al.*, eJSSNT **10**, 153 (2012); T. Okuda *et al.*, Rev. Sci. Inst. **82** (2011) 103302.

BL7B

## Filterless Vacuum Ultraviolet Photoconductive Detector Based on YF<sub>3</sub> Thin Film Prepared by Pulsed Laser Deposition

M. Yanagihara<sup>1</sup>, H. Ishikawa<sup>1</sup>, T. Tsuji<sup>1</sup>, H. Ohtake<sup>2</sup> and S. Ono<sup>1</sup>

<sup>1</sup> Nagoya Institute of Technology, Gokiso-cho, Showa-ku, Nagoya 466-8555, Japan

<sup>2</sup> Aisin Seiki Co., Ltd., 2-1 Asahi-machi, Kariya 448-8650, Japan

Due to potential applications such as monitoring for industrial processes and gas sensing, considerable attention has been focused on the development of vacuum ultraviolet (VUV) detectors. Currently, the study of photoconductive detectors using diamond, nitride, and oxide are demonstrated. However, these devices response deep-UV (DUV) range not only VUV range because of limitation by the band gap. Fluorides are relatively wide band gap in contrast to these materials[1, 2]. Here, we report on the development of VUV photoconductive detector, which has no sensitivity in DUV region without any filters, by utilizing the YF<sub>3</sub> thin films.

YF<sub>3</sub> thin film was grown by pulsed laser deposition (PLD) on the quartz glass substrate. YF<sub>3</sub> ceramic target was irradiated with the femtosecond laser pulses (wavelength: 790 nm, laser fluence: 13.5 J/cm<sup>2</sup>). Growth was carried out 3 h under high vacuum condition ( $2 \times 10^{-4}$  Pa). The substrate heating temperature was controlled at 670 K. Figure 1 is scanning electron microscope (SEM) images of YbF<sub>3</sub> thin film. A sub-micron-sized particulates make up the majority of the deposition layer. The thickness of the thin film was about 170 nm.

To evaluate these thin films as photoconductive detectors, a pair of interdigitated aluminum electrodes was fabricated onto the thin film by vacuum deposition. The patterned area of interdigitated electrodes was  $5 \times 4$  mm<sup>2</sup>. Both the gap between the electrodes and the width of the electrodes were 0.2 mm. In addition, we covered them with YF<sub>3</sub> thin film to prevent photoelectron emission from electrodes. Figure 2 shows I-V characteristic measured in the dark (unirradiation) and under illumination of VUV light from deuterium lamp (irradiation). The dark current was below 1 pA. The current value increased 3-digit before and after VUV illumination at an applied bias of 300 V.

To evaluate the spectral responsivity of the detector using YbF<sub>3</sub> thin film, a bias voltage of 200 V was applied to a pair of interdigitated electrodes. Photocurrent was measured at each wavelength of irradiative light from 100 to 300 nm. Figure 3 shows the results of the spectral responsivity evaluation combined with the transmission of the sample. It turned out that this detector responded only to VUV wavelengths shorter than 170-nm wavelength. The 170-nm wavelength corresponds to band gap of YbF<sub>3</sub>. Consequently, these results indicated that we developed a VUV photoconductive detector.

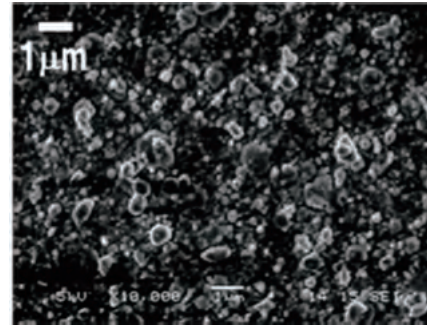


Fig. 1. SEM images of the surface and section of YbF<sub>3</sub> thin films.

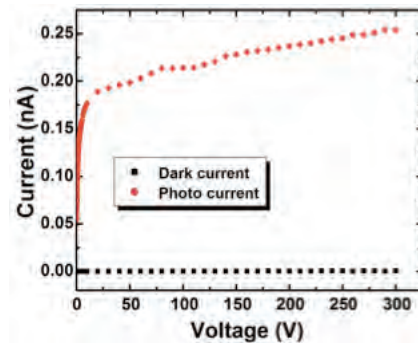


Fig. 2. I-V characteristic of YF<sub>3</sub> thin film.

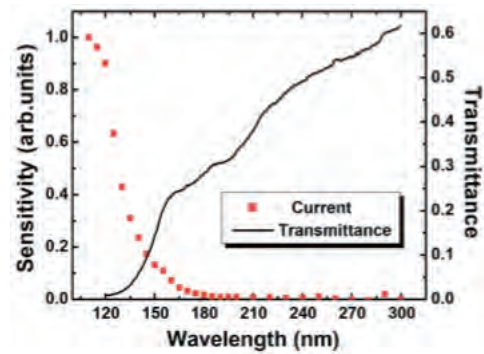


Fig. 3. Transmission spectrum and spectral response of the detector.

[1] M. Ieda, T. Ishimaru, S. Ono, K. Yamanoi, M. Cadatal, T. Shimizu, N. Sarukura, K. Fukuda, T. Suyama, Y. Yokota, T. Yanagida and A. Yoshikawa, *Jpn. J. Appl. Phys.* **51** (2012) 022603.

[2] T. Ishimaru, M. Ieda, S. Ono, Y. Yokota, T. Yanagida and A. Yoshikawa, *Thin Solid Films*, **534** (2013) 12-14.

BL8B

## ARUPS Study of Molecular Orientation of Pentacene Thin Film on SAM-Covered SiO<sub>2</sub>

K. K. Okudaira, N. Kanayama and N. Ueno

Association of Graduate Schools of Science and Technology, Chiba University,  
Chiba 263-8522, Japan

Field effect transistors (FETs) based on organic semiconducting materials have made rapid progress in recent years. Pentacene (Pn) is one of the best candidates for use in fabricating thin film transistors because of their high field effect charge mobility. A more efficient device is expected if all the molecules are packed orderly with the conducting channels in correct alignment relative to the electrodes. The self-assembled monolayers (SAMs) provide a systematic way to modify surface properties such as wetting and polarity of a substrate, which, in turn, may affect the orientation of a film deposited on top of it.

In this work we used methyl and phenyl group terminated SAMs for substrate and examined the molecular orientation of pentacene thin films crystals thermally deposited on these SAM surfaces by angle-resolved ultraviolet photoelectron spectroscopy (ARUPS) measurements. To obtain the quantitative analysis on the molecular orientation; we compare observed take-off angle dependence of  $\pi$  band and calculated ones by the independent-atomic-center (IAC)/MO approximation.

ARUPS measurements were performed at the beam line BL8B2 of the UVSOR storage ring at the Institute for Molecular Science. The take-off angle ( $\alpha$ ) dependencies of photoelectron spectra were measured at incident angle of photon ( $\theta$ ) = 45° with the photon energy ( $h\nu$ ) of 28 eV. We use octadecyltrichlorosilane (OTS) and trichloro(phenetyl)silane (phenyl) as coupling agent for SAM. The SAMs were prepared by dipping SiO<sub>2</sub> substrate at room temperatures. Pentacene thin film was deposited on these SAMs.

We observed take-off angle ( $\alpha$ ) dependence of HOMO peak in UPS of pentacene thin film (thickness of about 2.0 nm on OTS-SAM and 1.5nm on phenyl-SAM).

In Fig. 1 (a) the  $\alpha$  dependences of Pn(2.0nm)/OTS-SAM have a sharp maximum at  $\alpha=50^\circ$ , while  $\alpha$  dependences of Pn(1.5nm)/phenyl-SAM show two maxima at  $\alpha=50^\circ$  and  $20^\circ$ , which are different from those of Pn(2.0nm)/OTS-SAM. From the comparison with calculated results it is found that on the OTS-SAM pentacene molecules have stand-up orientation, while on the phenyl-SAM, pentacene molecules have not only stand-up orientation but also lie-flat orientation. This difference of film structure is responsible for the interaction between substrate

surface and molecules since the surface energy of OTS-SAM is smaller than that of phenyl-SAM.[1]

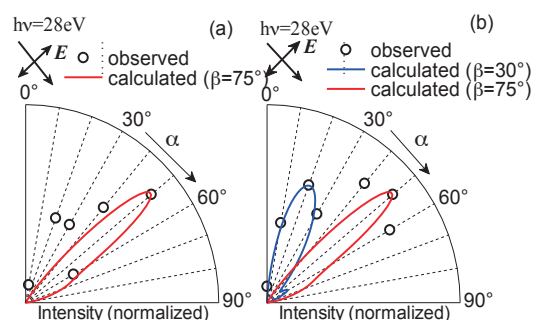


Fig. 1. Take-off angle ( $\alpha$ ) dependences of photoelectron intensities of HOMO peak of Pn(2.0nm)/OTS-SAM (a) and Pn(1.5nm)/phenyl-SAM (b). (—) and (---) : calculated  $\alpha$ -dependence for inclination angle ( $\beta$ ) = 75° and 30°.

[1] D. Janssen, *et al.*, *Thin. Solid. Films* **515** (2006) 1433.

BL8B

## Photoelectric Emission from Au on Zinc-Phthalocyanine Film

S. Tanaka<sup>1</sup>, T. Otani<sup>2</sup> and I. Hiromitsu<sup>2</sup>

<sup>1</sup> Department of Electric and Electronic Engineering, Faculty of Science and Engineering, Kinki University, Higashiosaka 577-8502, Japan

<sup>2</sup> Department of Physics and Materials Science, Graduate School of Science and Engineering, Shimane University, Matsue 690-8504, Japan

In general, the work function of thin films of metals and the ionization potential of organic thin films are no less than 4 eV. It is therefore expected that light energy of less than 4 eV cannot generate photoelectric emission from the surfaces of metal or organic films. However, we observed photoelectric emission from Ag on a zinc-phthalocyanine (ZnPc) layer at a photon energy of 3.4 eV. [1, 2] The threshold energy for this photoelectric emission is much smaller than the work function of Ag. Although the mechanism of this anomalous photoelectric emission is not clear, the previous results suggest that the vacuum level shift at the Ag/ZnPc interface play a key role. To investigate the mechanism of the anomalous photoelectric emission, we studied the photoelectric emission from Au on ZnPc film under UV-visible light irradiation.

The ZnPc was purchased from Kanto Chemical and sublimed three times for purification. ZnPc thin films were fabricated by vacuum deposition on a polycrystalline Ag substrate. The pressure used during the deposition was in the range of  $10^{-5}$  Pa. Au was used as the metal layer on the ZnPc film. The thicknesses of the ZnPc and Au were measured using a quartz microbalance. A white light source (a Xe lamp with an air mass 1.5 filter, HAL-320, Asahi Spectra Co. Ltd.) was used as UV-visible region light source. The UV-visible light was introduced to the measurement chamber through a glass viewport that cut off the light with wavelength shorter than approximately 320 nm. The power of the white light on the sample surface was  $100 \pm 10$  mW/cm<sup>2</sup>.

First, we fabricated the ZnPc thin film with the thickness of 10 nm. Under the white light irradiation, no photoelectric emission was observed from the ZnPc film as expected. The ionization potential of ZnPc film was estimated to be 5.0 eV by photoelectron spectroscopy using synchrotron radiation ( $h\nu = 39.6$  eV) (Fig. 1). On the other hand, in the case of the Au (0.2 nm)/ZnPc sample, we observed weak but obvious photoelectric emission under the white light irradiation. This is surprising since both of the work function of Au and the ionization potential of ZnPc are much larger than the highest energy of white light. Interestingly, no photoelectric emission under the white light irradiation was observed from the Au (1.0 nm)/ZnPc sample. In the case of Ag, the photoelectric emission under the white light irradiation was observed even at the Ag thickness of 20 nm.

Figure 1 shows the variation in the photoelectron spectrum of the ZnPc thin film (10 nm) during the incremental deposition of Au. The secondary cutoff was shifted toward higher kinetic energy by deposition of 1.0 nm Au. The HOMO peak of ZnPc (indicated by the bars in Fig. 1) showed a similar variation to that of the secondary electron cutoff. Vacuum level shift at metal/organic interfaces has been reported in many systems, and is attributed to the formation of an interfacial dipole layer. The direction and magnitude of interfacial dipole is affected by the work function of metal. Au has larger work function than Ag. Basically, the large work function of Au increases the threshold energy for the photoelectric emission. Indeed, the magnitude of the anomalous photoelectric emission on the Au/ZnPc surface under the white light irradiation was weaker than that on the Ag/ZnPc surface. However, the very small amount of Au on ZnPc surface caused the anomalous photoelectric emission. Further studies are needed to understand the role of Au and Ag in the anomalous photoelectric emission.

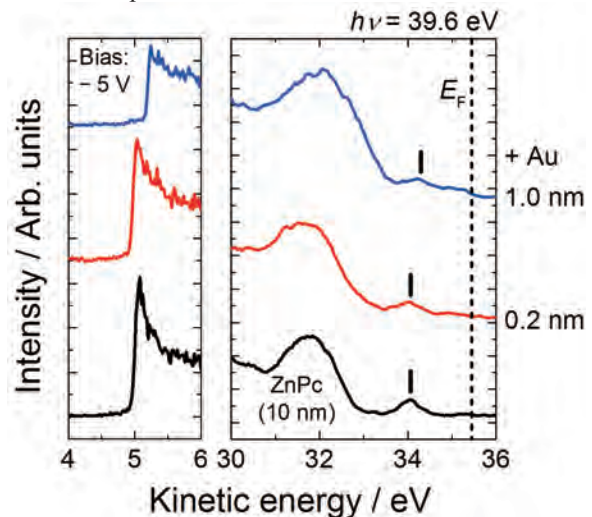


Fig. 1. Variation of the photoelectron spectra of the ZnPc film under incremental Au deposition (0.2, 1.0 nm). Left panel: Secondary electron cutoff region. The sample was biased at  $-5.0$  V during the measurements. Right panel: Around the Fermi level. No bias voltage was applied to the sample.

[1] S. Tanaka *et al.*, UVSOR Activity Report **40** (2013) 144.

[2] S. Tanaka *et al.*, submitted.

BL8B

## Electronic Structures of Organic Donor-Acceptor Interfaces of a Squaraine Dye and C<sub>60</sub>

Y. Nakayama<sup>1</sup>, K. R. Koswattage<sup>2</sup>, Y. Ozawa<sup>1</sup>, N. Ohashi<sup>3</sup> and H. Ishii<sup>1,2</sup>

<sup>1</sup>Graduate School of Advanced Integration Science, Chiba University, Chiba 263-8522, Japan

<sup>2</sup>Center for Frontier Science, Chiba University, Chiba 263-8522, Japan

<sup>3</sup>School of Engineering, Tohoku University, Sendai 980-8579, Japan

Squaraine dyes are recently attracting growing interest as promising donor materials for organic solar cell application owing to their efficient far red - near IR absorption [1, 2]. Kido *et al.* reported that blends of fullerenes with a member of the squaraine family, 2,4-bis[4-(N,N-di-isobutylamino)-2,6-dihydroxyphenyl] squaraine (SQ; see Fig. 1 inset), exhibited excellent solar cell efficiency [3]. In the present study, we investigated these organic donor-acceptor interfaces of SQ and C<sub>60</sub> fullerene by means of ultraviolet photoelectron spectroscopy (UPS).

SQ and C<sub>60</sub> were successively deposited onto indium-tin oxide (ITO) substrate pre-cleaned by ultrasonication followed by UV/O<sub>3</sub> treatment. UPS measurement was conducted at BL8B of UVSOR.

Firstly, we determined the ionization energy ( $I_s$ ) of SQ accurately. In this experiment, the excitation photon energy was carefully calibrated to be 29.76 eV by using the Fermi edge position of the second-order light. This allows one to decide the absolute value of the work function (WF) of the sample from the secondary electron cut-off (SECO) position. Figure 1 shows a UPS spectrum of a SQ film (5 nm-thick) plotted with respect to the vacuum level. Accordingly  $I_s$  value of SQ is settled to be 5.15 eV.

Figure 2 shows evolution of the UPS spectra of the C<sub>60</sub>-on-SQ and its reverse interfaces. For the former, stacking of C<sub>60</sub> lifted the vacuum level up as shown in Fig. 2(a), and the highest occupied molecular orbitals (HOMO) of both SQ and C<sub>60</sub> also shifted to the low binding energy (BE) side (Fig. 2(b)). In contrast, for the reverse interface (Fig. 2(c,d)), WF decreased on coverage of SQ over C<sub>60</sub>. The SQ HOMO exhibited the similar behavior to WF, while the C<sub>60</sub> HOMO stuck to its original position.

According to the UPS results, the energy level diagrams of the C<sub>60</sub>-on-SQ and SQ-on-C<sub>60</sub> interfaces can be drawn as shown in Fig. 3. Here the energy gap width of C<sub>60</sub> is assumed to be 2.3 eV [4]. The joint upward shift observed in the former system should be attributed to a band bending across the interface. Meanwhile, the downward shift of the vacuum level  $E_{vac}$  and SQ-HOMO apart from C<sub>60</sub> may be caused by orientation polarization of the SQ molecules [5].

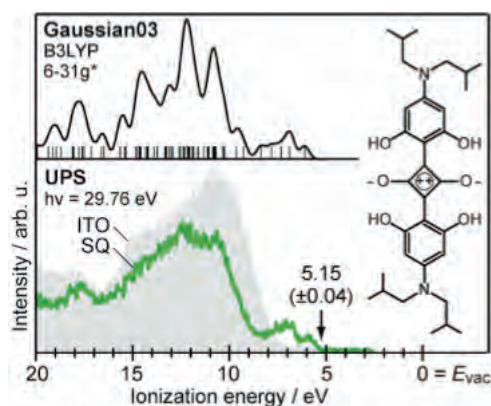


Fig. 1. UPS spectra of SQ film (5 nm) on ITO. A simulated density-of-states curve derived from the density functional theory calculation is also shown for reference. (Inset) The chemical structure of SQ.

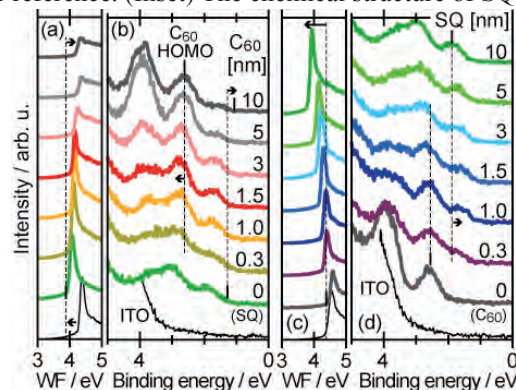


Fig. 2. Series of UPS spectra of (a,b) C<sub>60</sub>-on-SQ and (c,d) SQ-on-C<sub>60</sub> interfaces.

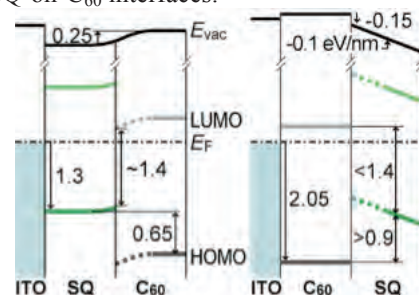


Fig. 3. Energy level diagrams of the (left) C<sub>60</sub>-on-SQ and (right) SQ-on-C<sub>60</sub> interfaces (units: eV).

- [1] K. Y. Law, Chem. Rev. **93** (1993) 449.
- [2] G. Wei *et al.*, ACS Nano **6** (2012) 972.
- [3] G. Chen *et al.*, Adv. Mater. **24** (2012) 2768; Appl. Phys. Lett. **101** (2012) 083904.
- [4] R. W. Lof *et al.*, Phys. Rev. Lett. **68** (1992) 3924.
- [5] Y. Nakayama *et al.*, Org. Electron. **13** (2012) 2850.

BL8B

## Efficiency of HATCN as a Hole Injection Layer in a Practical System

A. Yoneyama<sup>1</sup>, K. R. Koswattage<sup>2</sup>, Y. Nakayama<sup>1,3</sup> and H. Ishii<sup>1,2,3</sup>

<sup>1</sup>Faculty of Engineering, Chiba University, Chiba 263-8522, Japan

<sup>2</sup>Center for Frontier Science, Chiba University, Chiba 263-8522, Japan

<sup>3</sup>Graduate School of Advanced Integration Science, Chiba University, Chiba 263-8522, Japan

HATCN(dipyrazino[2,3-f:2',3'-h]quinoxaline-2,6,7,10,11-hexacarbonitrile) is known as a strong acceptor and actually has been reported to play a role of a hole injection layer in real devices [1]. Niederhausen et al clearly proved that this molecular layer actually lifted the highest occupied molecular orbital (HOMO) energies of ad-layers of several organic materials up toward the Fermi level of the metal substrate [2]. In this study, we examined how efficient the HATCN interlayer play a role of a hole injector in a more practical system ; that is HATCN on indium-tin oxide (ITO) substrates.

Clean ITO substrates were prepared through ultrasonication in acetone followed by UV/O<sub>3</sub> treatment. The work function of the ITO substrates was 4.3 - 4.4 eV. One-nanometer thick HATCN was then deposited at the evaporation rate of 0.1 nm/sec onto an ITO substrate to prepare a 'passivated ITO' substrate, which increased the work function of the substrate to 4.9 eV. C<sub>60</sub> was successively deposited onto the passivated and pristine (w/o HATCN) ITO substrates in a step-by-step manner up to 10 nm thick. All UPS spectra shown below were taken with the photon energy of 22 eV at BL-8B in UVSOR.

Figure 1 shows the evolutions of the UPS spectra in the secondary electron cut-off (SECO) region. On the pristine ITO the C<sub>60</sub> overlayer induced almost no vacuum level shift as seen in Fig. 1(a). Meanwhile, on the passivated ITO, one can find a downward vacuum level shift by 0.1eV as shown in Fig. 1(b).

Evolution of the valence band UPS spectra on growth of the C<sub>60</sub> overlayers is shown in Fig. 2. As each abscissa axis are taken with respect to the Fermi level, the onset binding energy of the HOMO peak corresponds to the hole injection barrier (HIB) from the electrode into C<sub>60</sub>. On the pristine ITO, the HOMO peak stayed at a constant energy position independent of the C<sub>60</sub> thickness (Fig. 2(a)). The HIB is estimated to be around 1.95eV for this case. On the other hand, as observed in Fig. 2(b), the HOMO peak of C<sub>60</sub> appeared at a smaller binding energy position on the HATCN interlayer; it emerged at the binding energy of 2.20 eV in the peak position, while it shifted further closer to the Fermi level by 0.15eV on growth to 2 nm or thicker. Accordingly, the HIB of C<sub>60</sub> on HATCN is determined to be 1.58eV from the HOMO position the 0.4 nm-thick overlayer, while the HOMO onset lifts up by 0.07 eV in the bulk region.

Figure 3 shows the energy level diagrams based on the values extracted from SECO/valence spectra and a literature [3]. C<sub>60</sub> on passivated ITO exhibited a 0.3eV lower HIB compared with the pristine ITO case. Also, in the passivated ITO case, band-bending

in the in the C<sub>60</sub> layer was observed toward the C<sub>60</sub>/HATCN interface, supposedly there are electric dipoles at the interface.

In summary, comparison of the UPS spectra between C<sub>60</sub>/HATCN/ITO and C<sub>60</sub>/ITO has revealed that insertion of the HATCN layer results in a 0.3eV lower HIB from ITO to C<sub>60</sub>. This supports that hole injection becomes advantageous by a HATCN interlayer in practical organic opto-electronic devices.

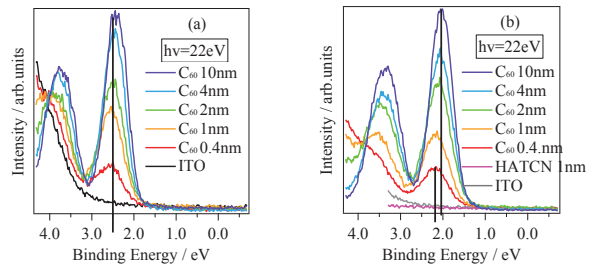


Fig. 1. UPS spectra in the SECO region of the C<sub>60</sub> overlayers on (a) pristine and (b) passivated ITO.

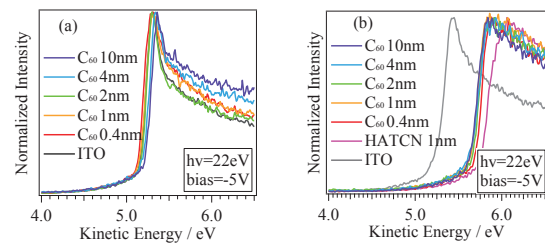


Fig. 2. UPS valence spectra of C<sub>60</sub> deposited onto the (a) pristine and (b)

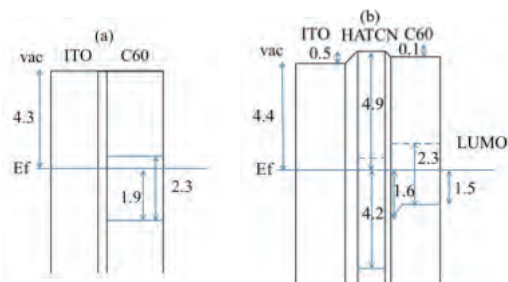


Fig. 3. Schematic energy level diagram for the deposition of C<sub>60</sub> on (a) pristine ITO and (b) passivated ITO. The value of the band gap of C<sub>60</sub> is taken from Ref.3.

[1] S. M. Park, Y. H. Kim, Y. Yi, H. Y. Oh and J. W. Kim, Appl. Phys. Lett. **97** (2010) 063308.

[2] J. Niederhausen *et al.*, Phys. Rev. B **84** (2011) 165302.

[3] R. W. Lof, *et al.*, Phys. Rev. Lett. **68** (1992) 3924.

BL8B

## HATCN on ITO: Work Function Variation and Influence of Air Exposure

K. R. Koswattage<sup>1</sup>, A. Yoneyama<sup>2</sup>, Y. Nakayama<sup>2</sup> and H. Ishii<sup>1,2</sup>

<sup>1</sup>Center for Frontier Science, Chiba University, Chiba, Japan

<sup>2</sup>Graduate School of Advanced Integration Science, Chiba University, Chiba, Japan,

HATCN (Hexaazatriphenylene-Hexanitrile) is used as an interlayer to increase the work function of metal electrodes for the application of organic electronics.

In this work, we mainly examined impact of air exposure on the valence electronic structure of HATCN prepared under UHV condition in order to evaluate its ionization potential (IP) because contradictory values are found in literatures and such discrepancy is likely to arise from variations in the experimental conditions. e.g. vacuum condition[1-3].

In this work, UPS measurements were done at BL8B, UVSOR. The excitation photon energy was carefully calibrated by using the Fermi edge energies of the first and second order light. ITO was cleaned by sequential ultra-sonication in acetone. The work function of the ITO substrate was determined to be 4.6 eV. Then, HATCN was subsequently deposited on the ITO, and a set of UPS measurements were performed at each step of the thickness.

Figure 1(a) shows the thickness-dependent UPS spectra of HATCN on ITO at the photon energy of 30 eV, and the top spectrum (dotted) of the Fig. 1(a) shows a calculated spectrum of HATCN using Gaussian. After about 1 nm, HOMO peak of HATCN can be distinguished from the O-2p feature of ITO and for the thickest film IP value of HATCN is estimated to be 9.1 eV. Kang *et al.* [3] performed similar works to investigate interface and molecular level alignment of HATCN on ITO and their results were almost consistent with our present findings. In Fig. 1(b), the work function change is plotted as a function of film thickness considering the energy position of the secondary energy cutoff (SECO; at -5 V sample bias). It is clear from the Fig. 1(b) that the work function can be controlled by HATCN.

To clarify the reason for the contradictory IP values of HATCN have been reported previously, we exposed this 10 nm-thick HATCN bulk film to the air in the dark for 12 h. The UPS measurements were subsequently performed and the results are shown in the Fig. 2. Figure 2(a) shows the HOMO region spectra before and after air exposure. The photon energy was set at 45 eV. Two additional features can be observed in the HOMO-LUMO gap region after air exposure. Considering the features separately, on-sets of them can be estimated as IP= 7.4 eV and 6.4 eV, while the original onset was IP = 9.1 eV. The value of 7.4 eV is consistent with the reported IP (7.5) by PYS [1] where the value might correspond to this gap states due to experimental condition of PYS. Further, it was observed that the SECO value changed to the low kinetic energy side after the air exposure as

shown in Fig. 2(b). Such changes should be essential to consider the application of HATCN for practical devices.

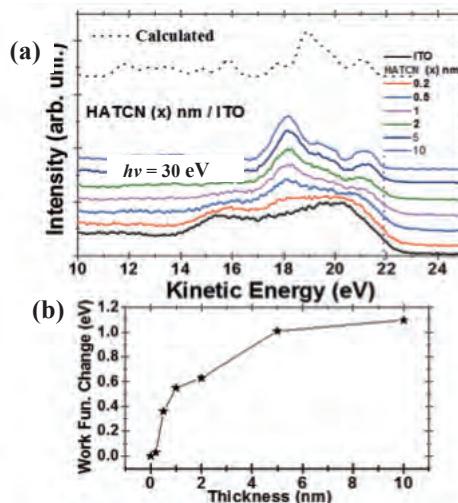


Fig. 1. (a) Thickness-dependent UPS of HATCN on ITO & simulated spectrum (top-dotted line). (b) Work function change of ITO as the function of HATCN thickness.

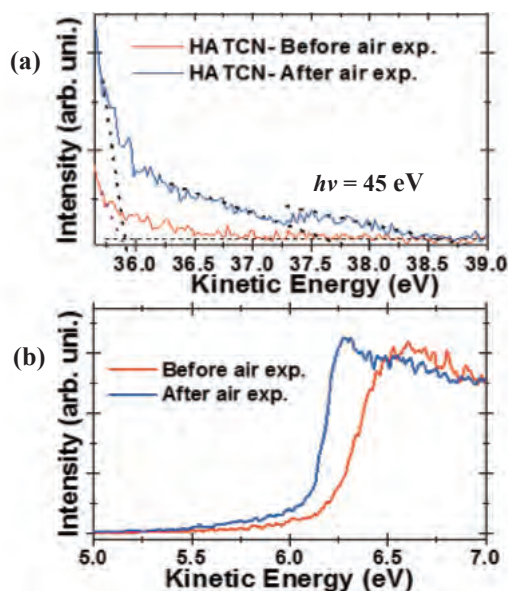


Fig. 2. UPS spectra of (a) HOMO and (b) SECO region before and after air exposure, respectively.

[1] T. Chiba *et al.*, *Org. Electron.* **12** (2011) 710.

[2] Y. K. Kim *et al.*, *Appl. Phys. Lett.* **94** (2009) 06330.

[3] H. Kang *et al.*, *J. Korean Phys. Soc.* **59** (2011) 3205.

BL8B

## Structural Requirements for the Charge-Transfer State Formation through Surface-Induced Aromatic Stabilization

T. Hosokai<sup>1</sup>, K. Yonezawa<sup>2</sup>, K. Kato<sup>2</sup>, R. Makino<sup>2</sup>, K. R. Koswattage<sup>2</sup>, N. Ueno<sup>2</sup> and S. Kera<sup>2</sup>

<sup>1</sup>Department of Materials Science and Technology, Iwate University, Morioka 020-8551, Japan

<sup>2</sup>Graduate School of Advanced Integration Science, Chiba 263-8522, Japan

Recently Heimel *et al.* and we found a new phenomenon occurred at  $\pi$ -conjugated organic molecules/noble metal interfaces, i.e., surface-induced aromatic stabilization (SIAS), and succeeded to explain a mechanism leading to a formation of charge-transfer (CT) states at the interfaces [1]. However, there still remain questions on the condition inducing SIAS. Here, we investigated a role of chemical structure on the SIAS by employing three kinds of polycyclic aromatic molecules, diindenoperylene (DIP:  $C_{32}H_{16}$ ), perylene ( $C_{20}H_{12}$ ) and picene ( $C_{22}H_{14}$ ), and angle-resolved ultraviolet photoelectron spectroscopy (UPS).

Figures 1(a) ~ 1(c) show the UPS results of DIP-monolayer (ML) on highly oriented pyrolytic graphite (HOPG), Ag(111) and Cu(111), perylene-ML on those substrates, and picene-ML and multilayer on Cu(111), respectively. All the measurements were performed at 295 K with the geometry illustrated in Fig. 1(d). The DIP (and perylene)/HOPG systems and the picene multilayer were measured for the reference of electronic structure at their physisorption, respectively. A lying-flat orientation was confirmed for all the monolayer systems by angular-dependence of photoelectron intensities (not shown). It is clear in Fig. 1(a) that DIP on Ag(111) and Cu(111) shows gap states (bold arrows), while other molecules do not (see Figs. 1(b) and 1(c)). As we discussed for DIP/Ag(poly) and Cu(poly) systems [2], the observed gap states for the DIP/Ag(111) and Cu(111) systems are attributed to CT states through SIAS due to electron transfers to the lowest unoccupied molecular orbital (LUMO) of the DIP monolayer from the substrates.

According to Ref. [1], the formation of CT states through SIAS requires a formation of *resonance state* of the adsorbate molecules; the resonance state brought by a site-specific substrate-molecule interaction reduces the LUMO binding energy, and results in the CT. As shown in Figs. 2(a) and 2(b), the DIP could have such a state, while its mother molecule, perylene, does not because, otherwise, two radicals remain at the center. However, as seen in Fig. 2(c) picene can also be drawn the entire resonance structure, although no CT state is observed in UPS (Fig. 1(c)). To ensure this, further experiments together with a theoretical calculation are strongly required.

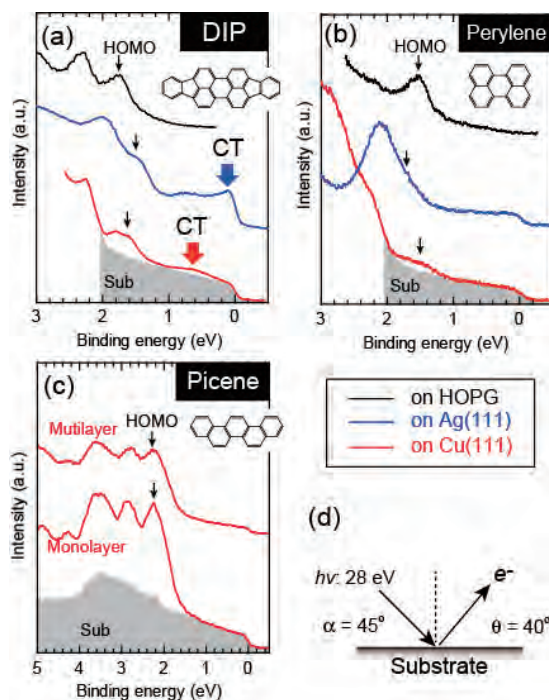


Fig. 1. Valence band structure of DIP-ML (a), perylene-ML (b), and picene-ML and -multilayer (c). Their chemical structure is depicted in each graph. The thin black arrows indicate the position of the highest-occupied molecular orbitals (HOMO). (d) The schematic at bottom right-hand side is the measurement geometry.

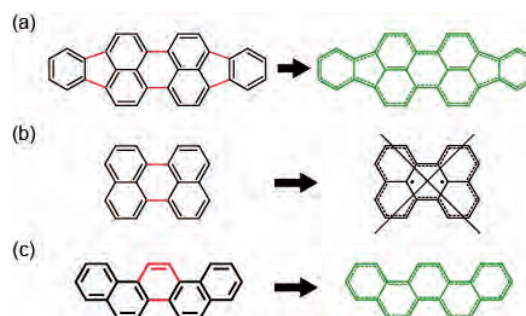


Fig. 2. A sketch of a resonance structure of DIP (a), perylene (b), and picene (c). All the molecules are connected with benzene and/or naphthalene rings (left, black lines).

[1] G. Heimel, *et al.*, Nature Chem. **5** (2013) 187.

[2] T. Hosokai, *et al.*, MRS proceedings, 1647 (2014) mrsf13-1647-gg01-03.